INT. J. NUM. METH. HEAT FLUID FLOW, VOL. 6, 31–58 (1996)

A SPECTRAL MULTIDOMAIN TECHNIQUE FOR THE COMPUTATION OF THE CZOCHRALSKI MELT CONFIGURATION

I. RASPO*, J. OUAZZANI** AND R. PEYRET***

*IRPHE, UMR 138, CNRS, IMFM 1, rue Honnorat, 13003 Marseille, France
**ArcoFluid, I. M. T. Technopôle de Château Gombert, 13451 Marseille, France
***Laboratoire de Mathématiques URA 168 C.N.R.S., Université de Nice-Sophia Antipolis, Parc Valrose-BP 71, 06108 Nice Cedex 2, France

ABSTRACT

This paper presents a spectral multidomain method for solving the Navier–Stokes equations in the vorticity-stream function formulation. The algorithm is based on an extensive use of the influence matrix technique and so leads to a direct method without any iterative process. Numerical results concerning the Czochralski melt configuration are reported and compared with spectral monodomain solutions to show the advantage of the domain decomposition for such a problem which solution presents a singular behaviour.

KEY WORDS Domain decomposition spectral methods Czochralski process

INTRODUCTION

The spectral methods have now evolved to a stage where their advantages and drawbacks have been well surrounded. They have in essence one of the major feature which any method should have in theory but are unfortunately lacking in many cases, which is in instance: "high accuracy". High accuracy can be achieved in classical methods (FV, FD, FE) by increasing essentially the mesh resolution and/or by introducing higher order schemes. However, the cost, in terms of memory and CPU, can be too excessive even for very powerful computers. It is one of the major reasons why spectral methods have been very attractive. They can be used very efficiently for calculating smooth solutions in rectangular domains with fewer nodes. This high accuracy may be lost however when the solution presents large gradients far from the boundaries or a singularity, for example due either to a discontinuity in the boundary conditions or to the geometry itself. Therefore, for such kind of problems, special treatments are necessary to recover either the "spectral accuracy" or, in the singular case, a sufficiently high precision. Some of these techniques are adaptive coordinate transformations[1,2] and domain decomposition[3–6].

We are interested here in the numerical approximation of solutions of the Navier–Stokes equations which exhibit a local singularity. The way considered is to use a domain decomposition technique in order to isolate the singularity at a corner of subdomains and to represent the solution in each subdomain by different Chebyshev polynomial approximations. The method is applied to the solution of the axisymmetric Navier–Stokes equations in the vorticity–stream function formulation coupled with an equation for the temperature and another for the azimuthal velocity. The algorithm is based on the influence matrix technique[7–10]. The aim of this approach is to obtain in a direct way, i.e. without iterative process, the values of the vorticity, the stream function, the azimuthal velocity and the temperature at the interface between two subdomains,

0961–5539/96/010031–28$2.00 *Received October 1994*

insuring the continuity of the normal derivatives of all variables. The values of the vorticity at the physical boundaries insuring the no-slip condition are obtained also through an influence matrix technique. When all these values are known, only independent Helmholtz equations with Dirichlet conditions have to be solved in each subdomain. Most of the Helmholtz problems involved in the method are time-independent and can be solved in a preprocessing stage before starting the time integration. The continuity influence matrix (CIM) and the boundary influence matrices (BIM) are also constructed and inverted once for all in the preprocessing stage.

The method described above has been applied to an industrial widely used crystal growth technique, more precisely the Czochralski crystal growth technique. This technique has been mainly used to obtain a large percentage of semiconductor crystals grown for the semiconductor industry. It is well documented in References 11 and 12. The modelling and understanding of heat and mass transfer have become an important issue in the optimisation of such a technique to grow more uniform and better quality crystals. The combination of natural convection due to thermal gradients between the crystal and the crucible and to forced convection due to rotation of the crystal and/or the crucible leads to problems which are complex in terms of the severity of the regimes developed inside such apparatus. Furthermore, the change in boundary conditions at the junction point between the crystal and the melt induces a singularity in the solution. The upper surface of the domain (*Figure 1*) presents two types of boundary condition for the velocity: noslip condition corresponding to the crystal interface and stress-free condition corresponding to the melt free surface. In some situations, the boundary conditions for the temperature can change also: the crystal interface is conducting while the melt surface is assumed to be adiabatic. In order to solve accurately this problem with spectral methods, the global domain has been decomposed into two subdomains where one subdomain lies below the crystal and the other below the melt free surface.

After describing the physical and mathematical problem of the Czochralski growth technique, we present the spatial and temporal discretizations for all equations and the algorithms for the monodomain method. Then we describe the behaviour of the boundary influence matrix for various types of configurations in a rectangular geometry. The multidomain algorithm is described thoroughly for the Stokes problem associated with the above physical problem and we discuss one of the original aspects of this paper which has been, besides the direct multidomain algorithm,

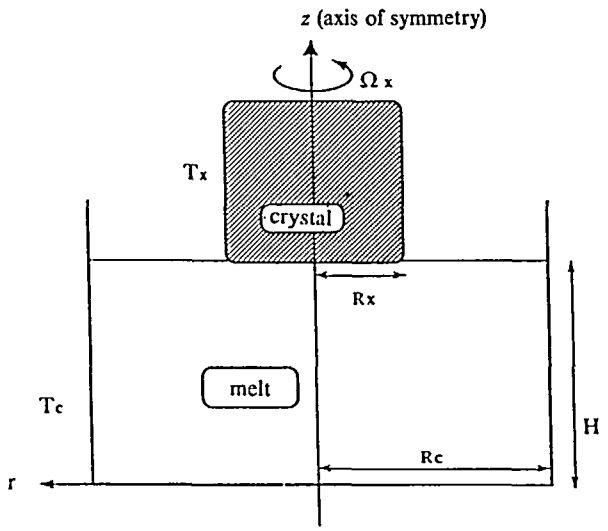

Figure 1 Geometrical configuration

the accurate handling with spectral methods of singularities arising at the physical boundaries of the computational domain. Then, a numerical comparison is made between the monodomain and the multidomain approaches and we show that the present multidomain technique allows the use of Chebyshev approximations without significant loss of accuracy.

PHYSICAL PROBLEM AND MODELLING

The physical model consists in a vertical cylinder of axis (0z), of radius R_c, filled with a melt until the height H. The free surface of the melt is partially limited by a crystal of radius R_x ($R_x < R_c$), which can be in rotation with the angular velocity Ω_x around the axis (0z) (see *Figure 1*). In practice, the crucible is generally also in rotation around its axis in the opposite direction of the crystal. However, we consider it unmoved in the limits of this paper.

Transient and steady laminar flows are considered with the assumption of axisymmetry. The fluid is initially at rest; then a difference of temperature is applied between the crystal and the crucible and/or the crystal rotates around its axis.

The governing equations are the Navier–Stokes equations within the Boussinesq approximation. We chose R_c as the characteristic length, ν/R_c as the characteristic velocity and R_c^2/ν as the characteristic time. The dimensionless physical parameters are:

$\alpha = \dfrac{H}{R_c}$ gap ratio

$\gamma = \dfrac{R_x}{R_c}$ radius ratio

$Re_x = \dfrac{2\Omega_x}{\nu} R_c^2$ Rotation Reynolds number of the crystal

$Pr = \dfrac{\nu}{\chi}$ Prandtl number

$Gr = \beta(T_c - T_0) g R_c^3/\nu^2$ Grashof number

where ν is the kinematic viscosity, g the gravity, χ the thermal diffusivity, β the thermal volume expansion coefficient, T_c the temperature of the crucible and T_0 the temperature of the crystal.

The dimensionless equations are:

$$\frac{\partial T}{\partial t} + u\frac{\partial T}{\partial r} + w\frac{\partial T}{\partial z} = \frac{1}{Pr}\Delta T, \tag{1}$$

$$\frac{\partial v}{\partial t} + u\frac{\partial v}{\partial r} + w\frac{\partial v}{\partial z} + \frac{uv}{r} = \Delta v - \frac{v}{r^2}, \tag{2}$$

$$\frac{\partial \omega}{\partial t} + u\frac{\partial \omega}{\partial r} + w\frac{\partial \omega}{\partial z} - \frac{u\omega}{r} = \Delta\omega - \frac{\omega}{r^2} + 2\frac{v}{r}\frac{\partial v}{\partial z} - Gr\frac{\partial T}{\partial r}, \tag{3}$$

$$\Delta'\psi - \omega r = 0, \tag{4}$$

where:

$$\Delta = \frac{\partial^2}{\partial r^2} + \frac{1}{r}\frac{\partial}{\partial r} + \frac{\partial^2}{\partial z^2}, \qquad \Delta' = \frac{\partial^2}{\partial r^2} - \frac{1}{r}\frac{\partial}{\partial r} + \frac{\partial^2}{\partial z^2}. \tag{5}$$

T is the temperature and v the azimuthal velocity. The vorticity ω is defined by:

$$\omega = \frac{\partial u}{\partial z} - \frac{\partial w}{\partial r}$$

and the stream function ψ is linked to the velocity components u and w by the formulas:

$$u = -\frac{1}{r}\frac{\partial \psi}{\partial z}, \qquad w = -\frac{1}{r}\frac{\partial \psi}{\partial r}.$$

These equations are solved with the following boundary conditions:

For the temperature T:

The vertical wall of the crucible is heated and its lower wall is adiabatic. The crystal is cold and a flux equal to zero is imposed on the axis. For the free surface of the melt, we suppose either a linear variation of temperature (case 1) or an adiabatic surface (case 2, only in the multidomain case). These conditions write:

$$T = 1 \qquad \text{for } r = 1 \text{ and } 0 \leqslant z \leqslant \alpha, \tag{6a}$$

$$\frac{\partial T}{\partial z} = 0 \qquad \text{for } 0 \leqslant r \leqslant 1 \text{ and } z = 0, \tag{6b}$$

$$T = 0 \qquad \text{for } 0 \leqslant r \leqslant \gamma \text{ and } z = \alpha, \tag{6c}$$

$$\frac{\partial T}{\partial r} = 0 \qquad \text{for } r = 0 \text{ and } 0 \leqslant z \leqslant \alpha, \tag{6d}$$

$$T = \frac{r-\gamma}{1-\gamma} \qquad \text{for } \gamma \leqslant r \leqslant 1 \text{ and } z = \alpha, \tag{6e}$$

$$\text{or } \frac{\partial T}{\partial z} = 0 \qquad \text{for } \gamma \leqslant r \leqslant 1 \text{ and } z = \alpha. \tag{6f}$$

For the azimuthal velocity v:

The azimuthal velocity v is equal to zero on the crucible walls and on the axis. On the crystal, v varies linearly with the radius and a stress-free condition is prescribed on the free surface. Therefore these conditions write:

$$v = 0 \qquad \text{for } r = 0 \text{ or } r = 1 \text{ and } 0 \leqslant z \leqslant \alpha, \text{ for } z = 0 \text{ and } 0 \leqslant r \leqslant 1, \tag{7a}$$

$$v = Re_x r \qquad \text{for } 0 \leqslant r \leqslant \gamma \text{ and } z = \alpha, \tag{7b}$$

$$\frac{\partial v}{\partial z} = 0 \qquad \text{for } \gamma \leqslant r \leqslant 1 \text{ and } z = \alpha. \tag{7c}$$

For (ω, ψ):

Noslip conditions are prescribed on the crucible walls and on the crystal. On the axis, we have the symmetry conditions and, on the free surface, the stress-free conditions. These conditions write for ω and ψ:

$$\psi = 0, \frac{\partial \psi}{\partial r} = 0 \qquad \text{for } r = 1 \text{ and } 0 \leqslant z \leqslant \alpha, \tag{8a}$$

$$\psi = 0, \frac{\partial \psi}{\partial z} = 0 \qquad \text{for } 0 \leqslant r \leqslant \gamma \text{ and } z = \alpha \text{ and for } 0 \leqslant r \leqslant 1 \text{ and } z = 0, \tag{8b}$$

$$\omega = 0, \psi = 0 \qquad \text{for } r = 0 \text{ and } 0 \leqslant z \leqslant \alpha \text{ and for } \gamma \leqslant r \leqslant 1 \text{ and } z = \alpha. \tag{8c}$$

Initial condition: The fluid is initially at rest:

$$u=0,\ w=0 \qquad \text{therefore } \omega=0, \tag{9a}$$

$$v=0 \tag{9b}$$

$$T=0 \qquad \text{for } 0\leqslant r\leqslant\gamma \text{ and } 0\leqslant z\leqslant\alpha, \tag{9c}$$

$$T=\frac{r-\gamma}{1-\gamma} \tag{9d}$$

$$\text{or } \frac{\partial T}{\partial z}=0 \qquad \text{for } \gamma\leqslant r\leqslant 1 \text{ and } 0\leqslant z\leqslant\alpha. \tag{9e}$$

NUMERICAL APPROXIMATION

Time-discretization

The time-discretization is done through the second order semi-implicit scheme introduced by Vanel *et al.*[8]. It is a three-level scheme with a fully implicit discretization of the diffusive terms and an Adams-Bashforth evaluation of the non-linear convective terms. It has been found by Ouazzani *et al.*[10] that such a scheme has good properties of stability. For the temperature equation, for example, it writes:

$$\frac{3T^{n+1}-4T^n+T^{n-1}}{2\delta t}+2\left(u\frac{\partial T}{\partial r}+w\frac{\partial T}{\partial z}\right)^n-\left(u\frac{\partial T}{\partial r}+w\frac{\partial T}{\partial z}\right)^{n-1}=\frac{1}{Pr}\Delta T^{n+1}. \tag{10}$$

For the azimuthal velocity and the vorticity equations, the equation obtained is similar except that the terms v/r^2 and ω/r^2 are also considered at level $n+1$. The scheme involving three time levels, the initialization requires a special treatment. Therefore, for the first time-step (that is $n=1$), we take:

$$\phi^{-1}=\phi^0 \qquad \text{for } \phi=\omega,\ T,\ v$$

that gives a first-order scheme.

Finally, with

$$\sigma_T=\frac{3}{2\,\delta t} \quad \text{and} \quad \sigma(r)=\frac{3}{2\,\delta t}+\frac{1}{r^2},$$

the equations to be solved at each time-cycle are:

$$\frac{1}{Pr}\Delta T^{n+1}-\sigma_T T^{n+1}=F_T^{(n,n-1)}(u, w, T), \tag{11}$$

$$\Delta v^{n+1}-\sigma(r)v^{n+1}=F_v^{(n,n-1)}(u, w, v), \tag{12}$$

$$\Delta\omega^{n+1}-\sigma(r)\omega^{n+1}=F_\omega^{(n+1,n,n-1)}(u, w, v, \omega, T), \tag{13}$$

$$\Delta'\psi^{n+1}-r\omega^{n+1}=0. \tag{14}$$

To these equations we must add the boundary conditions given in the previous section.

The temperature and the azimuthal velocity are calculated first and independently. Then, their values at level $n+1$ are included in the right hand side of the vorticity equation. And finally, the solution of the Stokes-type problem gives ω and ψ.

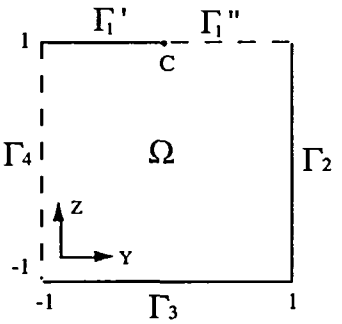

Figure 2 Computational domain for the monodomain case

Space-approximation

First, we use a coordinate transformation $(r, z)\rightarrow(Y, Z)$ to change the physical domain into the square domain $-1\leqslant Y, Z\leqslant 1$, in which the Chebyshev polynomials are defined. Each dependent variable is sought in the approximation space P_{NM}, composed by the polynomials of degree at most equal to N in the Y-direction and to M in the Z-direction. The collocation points, which are respectively the zeros of $(1-Y^2)T'_N(Y)$ and $(1-Z^2)T'_M(Z)$, are defined by:

$$Y_i=\cos\left(\frac{i\pi}{N}\right) \qquad \text{for } 0\leqslant i\leqslant N, \tag{15a}$$

$$Z_j=\cos\left(\frac{j\pi}{M}\right) \qquad \text{for } 0\leqslant j\leqslant M. \tag{15b}$$

By using these collocation points, the first order derivatives can be expressed by formulas of the type:

$$\frac{\partial}{\partial Y}\phi(Y_i, Z_j)=\sum_{k=0}^{N} d_Y^{(1)}(i, k)\phi(Y_k, Z_j). \tag{16}$$

The coefficients $d_Y^{(1)}(i, k)$ are expressed in the form of sinusoidal functions (see Appendix) which was found by Rothman[13] to reduce round-off errors. These formulas were also used by Ouazzani[14]. For the second order, the differentiation matrices are calculated from the square of the first order ones defined by (16). The nonlinear terms appearing in the right-hand-side of equations (11)–(14) are calculated through the pseudospectral technique making use of F.F.T algorithms.

At this point, we introduce some notations which will be used in the following sections. We note Γ the boundary of the domain Ω (see *Figure 2*): $\Gamma=\Gamma'_1\cup\Gamma''_1\cup\Gamma_2\cup\Gamma_3\cup\Gamma_4$. Let us note Ω_c the set of the collocation points inside the domain Ω:

$$\Omega_c=\{(Y_i, Z_j),\ 1\leqslant i\leqslant N-1,\ 1\leqslant j\leqslant M-1\},$$

and Γ_c the set of the collocation points belonging to the boundary Γ:

$$\begin{aligned}\Gamma_c&=\{(Y_i, 1),\ 0\leqslant i\leqslant N\}\cup\{(Y_i, -1),\ 0\leqslant \mathrm{i}\leqslant \mathrm{N}\}\cup\{(1, \mathrm{Z}_j),\ 0\leqslant \mathrm{j}\leqslant \mathrm{M}\}\cup\{(-1, \mathrm{Z}_j),\ 0\leqslant \mathrm{j}\leqslant \mathrm{M}\}\\&=\Gamma'_{1c}\cup\Gamma''_{1c}\cup\Gamma_{2c}\cup\Gamma_{3c}\cup\Gamma_{4c}.\end{aligned}$$

INFLUENCE MATRIX TECHNIQUE

The multidomain method developed in the present study is based on an extensive use of the well-known influence matrix technique considered in References 8 and 9 to handle the no-slip boundary conditions when solving the Stokes and Navier-Stokes equations. In order to make

clear the description of the multidomain method, we present in this section the influence matrix technique in the monodomain case. In particular, the important question concerning the rank of the influence matrix according to the type of boundary conditions will be pointed out.

Azimuthal velocity and temperature equations

The temperature and the azimuthal velocity equations are approximated using the collocation-Chebyshev method associated with a full matrix diagonalization. For the azimuthal velocity problem (or for the temperature problem when the free surface is adiabatic), the mixing of types of boundary conditions on the same side of the computational domain (Dirichlet condition on Γ_1' and Neumann condition on Γ_1'') led us to consider, as Pulicani[15], an influence matrix technique so that only Helmholtz problems with Dirichlet conditions have to be solved. Briefly, the solution is sought in the form:

$$v=\tilde{v}+\bar{v}, \tag{17}$$

where the part $\tilde{v}$ satisfies equation (12) with the boundary conditions (7a,b) and a homogeneous Dirichlet condition on Γ_1'' and the part $\bar{v}$ satisfies the homogeneous equation deduced from (12) with homogeneous boundary conditions instead of (7a,b). On the boundary Γ_1'', the part $\bar{v}$ is assumed to satisfy to the Dirichlet condition:

$$\bar{v}=\lambda,$$

where λ is unknown and must be determined so that the Neumann condition (7c) is satisfied. Let us note λ_k, $k=1, \ldots, K$, the values of λ at the K collocation points on Γ_1'' belonging to the segment $]Y_c, 1[$, where Y_c is the abscissa of the point C delimiting the crystal and the free surface. The solution $\bar{v}$ is sought in the form of the linear combination:

$$\bar{v}=\sum_{k=1}^{K}\lambda_k\bar{v}_k. \tag{18}$$

The elementary solution $\bar{v}_k$, $k=1, \ldots, K$, satisfies to the homogeneous equation deduced from (12) with homogeneous boundary conditions everywhere except on Γ_1'' where:

$$\bar{v}_k(Y_m, 1)=\delta_{km} \qquad \text{for } Y_m\in\Gamma_{1c}''$$

where δ_{km} is the Krönecker symbol. Now, by prescribing the Neumann condition (7c) satisfied by v at the collocation points on Γ_{1c}'', we obtain an algebraic system of K equations for the K unknowns, λ_k, $k=1, \ldots, K$.

Stokes-type problem

In this section, we consider the calculation of the vorticity and the stream function. For the sake of simplicity, we note ω, ψ for ω^{n+1}, ψ^{n+1}. At each time cycle, the following Stokes-type problem must be solved:

$$\begin{aligned} &\Delta\omega-\sigma(Y)\omega=F_\omega && \text{in } \Omega \\ &\Delta'\psi-(Y+1)\omega=0 && \text{in } \Omega, \end{aligned} \tag{19a}$$

$$\omega=0,\ \psi=0 \qquad \text{on } \Gamma_1''\cup\Gamma_4,$$

$$\psi=0,\ \frac{\partial\psi}{\partial Y}=0 \qquad \text{on } \Gamma_2, \tag{19b}$$

$$\psi=0,\ \frac{\partial\psi}{\partial Z}=0 \qquad \text{on } \Gamma_1'\cup\Gamma_3,$$

where Δ and Δ' are the Laplacian-type operators (5) expressed in variables Y and Z.

The main drawback of the vorticity-stream function formulation is the existence of two boundary conditions for the stream function ψ (a Dirichlet condition and a Neumann condition) and none boundary condition for the vorticity ω on noslip walls (Γ'_1, Γ_2 and Γ_3). On the other hand, ψ and ω are given on the boundaries Γ''_1 and Γ_4 where $\psi=0$, $\omega=0$. The difficulty associated with the noslip conditions is removed by using the influence matrix technique[8,9]. The method consists of seeking the solution in the form:

$$\begin{aligned} \omega &= \tilde{\omega}+\bar{\omega}, \\ \psi &= \tilde{\psi}+\bar{\psi}. \end{aligned} \tag{20}$$

The pair $(\tilde{\omega}, \tilde{\psi})$ satisfies the equations (19a) with the given Dirichlet boundary conditions for ψ. On the boundaries where ω is unknown, we impose a homogeneous Dirichlet condition for ω. The problem $\tilde{P}$ to be solved is, therefore:

$$\begin{aligned} &\Delta\tilde{\omega}-\sigma(Y)\tilde{\omega}=F_\omega && \text{in } \Omega, \\ &\tilde{\omega}=0 && \text{on } \Gamma, \\ &\Delta'\tilde{\psi}=(Y+1)\tilde{\omega} && \text{in } \Omega, \\ &\tilde{\psi}=0 && \text{on } \Gamma. \end{aligned} \tag{21}$$

This problem, consisting in two successive Dirichlet problems for a Helmholtz or Poisson equation, is solved using the Chebyshev-collocation method associated with a full matrix diagonalization.

The pair $(\bar{\omega}, \bar{\psi})$ satisfies to the homogeneous equations deduced from (19a) with homogeneous Dirichlet boundary conditions for $\bar{\psi}$. On the boundaries where ω is given, we impose $\bar{\omega}=0$ and on the other boundaries, its unknown value $\bar{\omega}=\lambda$ has to be determined so that the Neumann condition for ψ is satisfied. This defines the problem $\bar{P}$:

$$\begin{aligned} &\Delta\bar{\omega}-\sigma(Y)\bar{\omega}=0 && \text{in } \Omega, \\ &\Delta'\bar{\psi}-(Y+1)\bar{\omega}=0 && \text{in } \Omega \\ &\bar{\omega}=0 && \text{on } \Gamma-\Gamma^*=\Gamma''_1\cup\Gamma_4, \\ &\bar{\omega}=\lambda && \text{on } \Gamma^*=\Gamma'_1\cup\Gamma_2\cup\Gamma_3, \\ &\Delta'\bar{\psi}=(Y+1)\bar{\omega} && \text{in } \Omega, \\ &\bar{\psi}=0 && \text{on } \Gamma. \end{aligned} \tag{22}$$

Then, the solution $(\bar{\omega}, \bar{\psi})$ of the above problem is looked for in the form:

$$\begin{aligned} \bar{\omega} &= \sum_{k=1}^{K} \lambda_k\bar{\omega}_k, \\ \bar{\psi} &= \sum_{k=1}^{K} \lambda_k\bar{\psi}_k, \end{aligned} \tag{23}$$

where each pair $(\bar{\omega}_k, \bar{\psi}_k)$, for $k=1, \ldots, K$, is solution of the problem $\bar{P}_k$:

$$\begin{aligned} &\Delta\bar{\omega}_k-\sigma(Y_j)\bar{\omega}_k=0 && \text{in } \Omega_c, \\ &\bar{\omega}_k=0 && \text{on } \Gamma_c-\Gamma_c^*, \\ &\bar{\omega}_k(\eta_m)=\delta_{km} && \text{for } \eta_m=(Y_m, Z_m)\in\Gamma_c^*, \\ &\Delta'\bar{\psi}_k=(Y_j+1)\bar{\omega}_k && \text{in } \Omega_c, \\ &\bar{\psi}_k=0 && \text{on } \Gamma_c. \end{aligned} \tag{24}$$

We note that the problem $\bar{P}$ like the problem $\tilde{P}$ reduces to the solution of successive Helmholtz

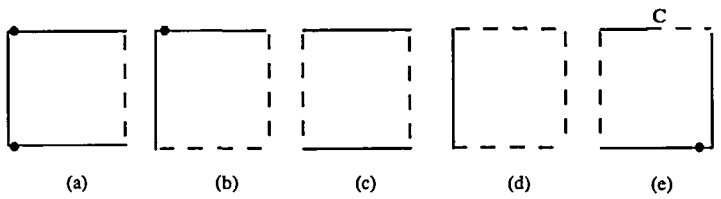

Figure 3 Various configurations of boundary conditions, full line: noslip condition ($\psi = 0, \partial\psi/\partial n = 0$), dash line: stress-free condition ($\psi = 0, \omega = 0$) (the dots figure the removed points)

Table 1 Number of null eigenvalues of the influence matrix

Case	(a)	(b)	(c)	(d)
n	2	1	0	0
K	$2N+M-5$	$N+M-3$	$2N-2$	$M-1$

equations for the vorticity and the stream function with Dirichlet boundary conditions. In (24), the set Γ_c^* is composed by K collocation points belonging to the boundaries Γ_1', Γ_2, Γ_3. The convenient value of K, i.e. the precise definition of Γ_c^*, is discussed below.

The parameters λ_k, $k=1, \ldots, K$, in (23) are the values of the function λ at the collocation points η_m belonging to Γ_c^*. These parameters are determined so that the Neumann condition for ψ on the boundary Γ_c^* is satisfied. Hence, we obtain an algebraic system of K equations for the K unknowns λ_k, $k=1, \ldots, K$, whose matrix is called the boundary influence matrix (BIM).

The rank of the BIM, that is the number K, has been studied in References 9 and 16 for the case where noslip conditions are prescribed on the whole boundary. It was found to be equal to $2N+2M-8$: the four corners and four supplementary points must be removed. A possible choice for the last four points to be removed consists in the points $(Y_1, 1)$, $(Y_{N-1}, 1)$, $(Y_1, -1)$ and $(Y_{N-1}, -1)$. Another possible choice is given by the points $(Y_{N-1}, 1)$, $(1, Z_1)$, $(Y_1, -1)$ and $(-1, Z_{M-1})$. However, the choice is not completely arbitrary. A systematic study of the convenient location of the points to be removed is done in Reference 16. It can be shown that the noslip condition is satisfied at the removed points although it is not explicitly prescribed. The proof is based on the compatibility relations of polynomials at the corners. Incidentally, concerning the elimination of the corners, it must be pointed out that, for the second-order differential problems without crossed derivatives like (5), the values of the unknowns at the corners are not involved in the collocation Chebyshev approximation.

Theoretical and numerical studies have been done also for cases where some part of the boundary conditions are noslip and others are stress-free. Let us consider, for example, the configurations represented in *Figure 3*. Numerical experiments of Chaouche[17] and mathematical arguments of Bwemba and Pasquetti[18] have determined the number of points to be removed for the configurations (a), (b), (c) and (d). The number of points (in addition to the corners) to be eliminated is equal to the number n of the BIM eigenvalues equal to zero. We give this number and the rank K of the BIM for each configuration in *Table 1*.

The rule to determine the number of null eigenvalues (after removing the corners) is simple. In the cases (a)–(d), there is a zero eigenvalue attached to a corner if and only if both adjacent sides are noslip walls. The choice of the points to be removed is not indifferent, in particular the location of the eliminated points influences the condition number of the BIM. The most performing choice, represented on *Figure 3*, corresponds to points removed near the corner associated with the zero eigenvalue.

For the problem treated in this paper, configuration (e), the point C acts like a corner between two sides with a change of boundary conditions. Therefore, none zero eigenvalue is attached to

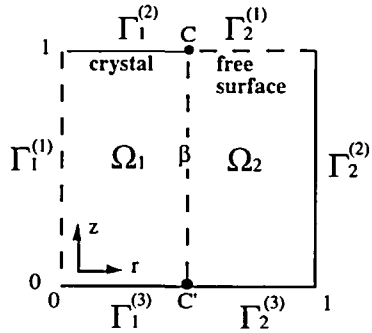

Figure 4 Computational domain for the two-domains case.

this point and only one supplementary point must be removed (a zero eigenvalue attached to the corner $(1, -1)$). We noted that a good condition number is obtained by removing the point $(Y_1, -1)$ or the point $(1, Z_{M-1})$. We chose here to eliminate the point $(Y_1, -1)$.

Finally, it must be noticed that the influence matrix method does not give the values of the vorticity at a noslip wall[9]. These values, which are needed for the evaluation of the convective term, are calculated by using the stream function equation written at the wall.

The numerical results obtained for the Czochralski problem using the above described monodomain method will be discussed later. The discontinuity of the boundary conditions at the junction crystal-free surface produces a singularity in the vorticity, in the azimuthal velocity derivative and in the temperature one in the case of condition (6f). These singularities induce oscillations in the computed solutions which cannot be removed by increasing the resolution. In the following section, a two-domain decomposition method will be considered in order to isolate the singularity at a corner of the computational domain. In such a situation, the solution in each subdomain is singular at this corner and its polynomial approximation, different in each subdomain, is found to be free of oscillations.

MULTIDOMAIN SOLUTION

The basic problem is formed by the equations (11)–(14) with the boundary conditions (6)–(8). The multidomain method consists of splitting the computational domain Ω into two subdomains (Ω_1 which contains the boundary of the crystal and Ω_2 which contains the free surface of the melt, see *Figure 4*), in which the polynomial approximation in the radial direction may be of different degree. Then, the global problem is replaced by a set of two independent problems which solutions are coupled by imposing the continuity of the dependent variables and of their first-order normal derivative at the interface, β, between the two adjacent subdomains:

$$\phi_1 = \phi_2, \qquad \frac{\partial \phi_1}{\partial r} = \frac{\partial \phi_2}{\partial r} \qquad \text{on } \beta, \tag{25}$$

for $\phi = \omega, \psi, T, v$. The subscript 1 refers to the solution in Ω_1 and the subscript 2 refers to this in Ω_2. These conditions of continuity are satisfied using again the influence matrix technique.

Stokes-type problem

In this section, we present the fundamentals of the method to solve the Stokes-type problem for (ω, ψ). The solution method of the Helmholtz problems determining the azimuthal velocity v and the temperature T will follow the same main outlines with obvious simplifications.

Let (ω_i, ψ_i) be the solution of the Stokes-type problem in the subdomain Ω_i, $i=1, 2$. It is divided into two parts:

$$\omega_i=\tilde{\omega}_i+\bar{\omega}_i, \qquad \psi_i=\tilde{\psi}_i+\bar{\psi}_i, \qquad i=1, 2. \tag{26}$$

The first part $(\tilde{\omega}_i, \tilde{\psi}_i)$ satisfies to the Stokes equations (13)–(14), the physical boundary conditions (8) and homogeneous Dirichlet conditions on the interface. The second part $(\bar{\omega}_i, \bar{\psi}_i)$, satisfies to the homogeneous equations deduced from (13)–(14) and homogeneous physical boundary conditions. Their values at the interface β are unknown: they are found by prescribing the continuity of the normal derivatives at the interface.

More precisely, the pairs $(\tilde{\omega}_i, \tilde{\psi}_i)$, $i=1, 2$, are solutions of:

*Problem $\tilde{P}_1$:

$$\begin{aligned}
&\Delta_1\tilde{\omega}_1-\sigma_1\tilde{\omega}_1=F_{\omega_1} && in\,\Omega_1,\\
&\Delta_1'\tilde{\psi}_1-\gamma(Y+1)\tilde{\omega}_1=0 && \text{in } \Omega_1,\\
&\tilde{\omega}_1=0,\ \tilde{\psi}_1=0 && \text{on } \Gamma_1^{(1)},\\
&\tilde{\psi}_1=0,\ \frac{\partial\tilde{\psi}_1}{\partial Z}=0 && \text{on } \Gamma_1^{(2)}\cup\Gamma_1^{(3)},\\
&\tilde{\omega}_1=0,\ \tilde{\psi}_1=0 && \text{on } \beta.
\end{aligned} \tag{27}$$

*Problem $\tilde{P}_2$:

$$\begin{aligned}
&\Delta_2\tilde{\omega}_2-\sigma_2\tilde{\omega}_2=F_{\omega_2} && in\,\Omega_2,\\
&\Delta_2'\tilde{\psi}_2-(1-\gamma)(Y+\chi)\tilde{\omega}_2=0 && \text{in } \Omega_2,\\
&\tilde{\omega}_2=0,\ \tilde{\psi}_2=0 && \text{on } \Gamma_2^{(1)},\\
&\tilde{\psi}_2=0,\ \frac{\partial\tilde{\psi}_2}{\partial Y}=0 && \text{on } \Gamma_2^{(2)},\\
&\tilde{\psi}_2=0,\ \frac{\partial\tilde{\psi}_2}{\partial Z}=0 && \text{on } \Gamma_2^{(3)},\\
&\tilde{\omega}_2=0,\ \tilde{\psi}_2=0 && \text{on } \beta,
\end{aligned} \tag{28}$$

where $\chi=(1+\gamma)/(1-\gamma)$ and Δ_i and Δ_i' the operators (5) expressed in variables Y, Z in the subdomain Ω_i.

The pairs $(\bar{\omega}_i, \bar{\psi}_i)$, $i=1, 2$, are solutions of:

*Problem $\bar{P}_1$:

$$\begin{aligned}
&\Delta_1\bar{\omega}_1-\sigma_1\bar{\omega}_1=0 && in\,\Omega_1\\
&\Delta_1'\bar{\psi}_1-\gamma(Y+1)\bar{\omega}_1=0 && \text{in } \Omega_1,\\
&\bar{\omega}_1=0,\ \bar{\psi}_1=0 && \text{on } \Gamma_1^{(1)},\\
&\bar{\psi}_1=0,\ \frac{\partial\bar{\psi}_1}{\partial Z}=0 && \text{on } \Gamma_1^{(2)}\cup\Gamma_1^{(3)},\\
&\bar{\omega}_1=\lambda,\ \bar{\psi}_1=\mu && \text{on } \beta.
\end{aligned} \tag{29}$$

*Problem $\bar{P}_2$:

$$\begin{aligned}
&\Delta_2\bar{\omega}_2-\sigma_2\bar{\omega}_2=0 && \text{in}\,\Omega_2,\\
&\Delta_2'\bar{\psi}_2-(1-\gamma)(Y+\chi)\bar{\omega}_2=0 && \text{in}\ \Omega_2,\\
&\bar{\omega}_2=0,\ \bar{\psi}_2=0 && \text{on}\ \Gamma_2^{(1)},\\
&\bar{\psi}_2=0,\ \frac{\partial\bar{\psi}_2}{\partial Y}=0 && \text{on}\ \Gamma_2^{(2)},\\
&\bar{\psi}_2=0,\ \frac{\partial\bar{\psi}_2}{\partial Z}=0 && \text{on}\ \Gamma_2^{(3)},\\
&\bar{\omega}_2=\lambda,\ \bar{\psi}_2=\mu && \text{on}\ \beta.
\end{aligned} \tag{30}$$

The two uncoupled problems (27)–(28) are Stokes-type problems. They are solved using the monodomain influence matrix technique described previously. The rank of the influence matrix of each problem is determined by the type of boundary conditions as considered in *Figure 3*. Therefore, the solution in Ω_1 corresponds to the configuration (c) and the solution in Ω_2 to the configuration (b).

The problems (29)–(30) are coupled by the unknown values λ and μ at the interface β. These values will be determined by requiring the continuity of the normal derivative of ω and ψ through β. This is done using again an influence matrix technique. The pairs $(\bar{\omega}_i, \bar{\psi}_i)$, $i=1,2$, are sought in the form of a linear combination involving $2K$ parameters:

$$\begin{aligned}
\bar{\omega}_i&=\sum_{k=1}^{K}\lambda_k\bar{\omega}_{ik}'+\sum_{k=1}^{K}\mu_k\bar{\omega}_{ik}'',\\
\bar{\psi}_i&=\sum_{k=1}^{K}\lambda_k\bar{\psi}_{ik}'+\sum_{k=1}^{K}\mu_k\bar{\psi}_{ik}''.
\end{aligned} \tag{31}$$

where K is the number of interior collocation points on the interface β.

For $k=1, \ldots, K$, the pairs $(\bar{\omega}_{1k}', \bar{\psi}_{1k}')$ and $(\bar{\omega}_{1k}'', \bar{\psi}_{1k}'')$ satisfy to problems of type $\bar{P}_1$ with, on the interface, a non null boundary condition either for the vorticity or for the stream function. More precisely, the problems to solve are:

*Problem $\bar{P}_{1k}'$ in Ω_1:

$$\begin{aligned}
&\Delta_1\bar{\omega}_{1k}'-\sigma_1\bar{\omega}_{1j}'=0 && \text{in}\,\Omega_{1c}\\
&\Delta_1'\bar{\psi}_{1k}'-\gamma(Y_j+1)\bar{\omega}_{1k}'=0 && \text{in}\ \Omega_{1c}\\
&\bar{\omega}_{1k}'=0,\ \bar{\psi}_{1k}'=0 && \text{on}\ \Gamma_{1c}^{(1)}\\
&\bar{\psi}_{1k}'=0,\ \frac{\partial\bar{\psi}_{1k}'}{\partial Z}=0 && \text{on}\ \Gamma_{1c}^{(2)}\cup\Gamma_{1c}^{(3)}\\
&\bar{\omega}_{1k}'(\eta_m)=\delta_{km},\ \bar{\psi}_{1k}'(\eta_m)=0 && \text{for}\ \eta_m=(1, Z_m)\in\beta_c
\end{aligned} \tag{32}$$

*Problem $\bar{P}_{1k}''$ in Ω_1:

$$\begin{aligned}
&\Delta_1\bar{\omega}_{1k}''-\sigma_1\bar{\omega}_{1k}''=0 && \text{in}\,\Omega_{1c}\\
&\Delta_1'\bar{\psi}_{1k}''-\gamma(Y_j+1)\bar{\omega}_{1k}''=0 && \text{in}\ \Omega_{1c}\\
&\bar{\omega}_{1k}''=0,\ \bar{\psi}_{1k}''=0 && \text{on}\ \Gamma_{1c}^{(1)},\\
&\bar{\psi}_{1k}''=0,\ \frac{\partial\bar{\psi}_{1k}''}{\partial Z}=0 && \text{on}\ \Gamma_{1c}^{(2)}\cup\Gamma_{1c}^{(3)},\\
&\bar{\omega}_{1k}''(\eta_m)=0,\ \bar{\psi}_{1k}''(\eta_m)=\delta_{km} && \text{for}\ \eta_m=(1, Z_m)\in\beta_c.
\end{aligned} \tag{33}$$

So the set of solutions built is linearly independent. Here again each problem $\bar{P}'_{1k}$ and $\bar{P}''_{1k}$ is a Stokes-type problem solved using the monodomain influence matrix technique. In Ω_2, the pairs $(\bar{\omega}'_{2k}, \bar{\psi}'_{2k})$ and $(\bar{\omega}''_{2k}, \bar{\psi}''_{2k})$, for $k=1, \ldots, K$, satisfy to the same type of equations with the same conditions on the interface except, of course, for the physical boundary conditions (problems $\bar{P}'_{2k}$ and $\bar{P}''_{2k}$).

We note that, taking the boundary conditions for $\bar{\omega}'_{1k}$, $\bar{\psi}'_{1k}$, $\bar{\omega}''_{1k}$ and $\bar{\psi}''_{1k}$ into account, the parameters λ_k and μ_k are respectively the values of the functions λ and μ, introduced in (29)–(30), at the collocation points η_k of the interface. These parameters are determined so that the continuity of the normal derivatives at the interface β is satisfied. Taking the decompositions (26) and (31) into account, we obtain an algebraic system of $2K$ equations for the $2K$ parameters λ_k, μ_k, for $k=1, \ldots, K$. This system writes:

$$\begin{bmatrix} \mathbf{A}_{11} & \mathbf{A}_{12} \\ \mathbf{A}_{21} & \mathbf{A}_{22} \end{bmatrix} \begin{pmatrix} \Lambda \\ \mathbf{M} \end{pmatrix} = \begin{pmatrix} H \\ G \end{pmatrix} \tag{34}$$

where $\Lambda=[\lambda_1, \ldots, \lambda_K]^T$ and $\mathbf{M}=[\mu_1, \ldots, \mu_K]^T$. The matrix A defined by:

$$\mathbf{A}=\begin{bmatrix} \mathbf{A}_{11} & \mathbf{A}_{12} \\ \mathbf{A}_{21} & \mathbf{A}_{22} \end{bmatrix} \tag{35}$$

is the influence matrix called here the continuity influence matrix (CIM). This matrix is also often called 'capacitance matrix'[19]. Each block A_{nm} is a square matrix $K \times K$ which depends only on one type of elementary solution $\bar{\omega}'_{ik}$, $\bar{\psi}'_{ik}$, $\bar{\omega}''_{ik}$ or $\bar{\psi}''_{ik}$, $i=1, 2$, $k=1, \ldots, K$. Since these elementary solutions are time-independent, the matrix A is time-independent. The rank of each square submatrix $\mathbf{A}_{nm}$ is $K=M-2$. The two extreme points of the interface β are removed since they are corners of subdomains. However, the values of ω and ψ are known at these two points. At point C (see *Figure 4*), ψ is equal to zero (given boundary condition) and ω is either calculated by the stream function equation on the crystal (domain Ω_1) or equal to zero on the free surface (domain Ω_2). At point C′ (see *Figure 4*), ψ is equal to zero (given boundary condition) and ω is calculated by the stream function equation.

We must note that, since the continuity of normal derivatives is not imposed at these two points, the Neumann boundary condition for ψ is not explicitely prescribed at point C′. In fact, it can be proved[20] that, since this condition is satisfied on all the other points of the boundaries $\Gamma_1^{(3)}$ and $\Gamma_2^{(3)}$, it is also satisfied at this point.

A constant and important question when dealing with Chebyshev polynomial approximations is the conditioning of the associated matrices, which may be deteriorated when the resolution increases. The condition number (as given by the subroutine EPIRG of IMSL library) of the various influences matrices is given in *Table 2* (effect of the time step) and in *Table 3* (effect of the resolution). It may be seen that the BI matrices $\mathbf{M}_1$ (associated with the subdomain Ω_1) and M_2 (associated with Ω_2) have relatively good condition numbers. The same is true for the *CI* matrices A_v and A_T associated respectively with the azimuthal velocity and temperature solutions.

Table 2 Time-step effect on the condition number of the influence matrices for $N \times M = 41 \times 41$, with $N_1 = N_2 = (N+1)/2$ in the two-domain case

δt	10^{-2}	5×10^{-5}	5×10^{-6}
M_1	5.78×10^{-2}	1.47×10^{-1}	1.73×10^{-1}
M_2	5.75×10^{-2}	1.29×10^{-1}	5.83×10^{-2}
A_v	10^{-1}	8.91×10^{-2}	1.61×10^{-1}
A_T	7.99×10^{-2}	5.91×10^{-2}	6.26×10^{-2}
A	$8{,}02 \times 10^{-6}$	1.04×10^{-5}	1.13×10^{-5}
PA	2.91×10^{-1}	4.43×10^{-1}	2.27×10^{-1}

Table 3 Resolution effect on the condition number of the influence matrices for $\delta t = 5 \times 10^{-6}$

N × M	41 × 41	55 × 41	55 × 61
M_1	1.73×10^{-1}	2.09×10^{-1}	1.53×10^{-1}
M_2	5.83×10^{-2}	9.11×10^{-2}	5.34×10^{-2}
A_v	1.61×10^{-1}	1.06×10^{-1}	1.07×10^{-1}
A_T	6.26×10^{-2}	7.54×10^{-2}	6.33×10^{-2}
A	1.13×10^{-5}	1.90×10^{-5}	1.55×10^{-5}
PA	2.91×10^{-1}	3.57×10^{-1}	2.58×10^{-1}

On the other hand, the *CI* matrix A associated with the Stokes problem, which is a large matrix $2K \times 2K$, is generally ill-conditioned. This is due to a bad balance between its coefficients. In fact, the elements of the two diagonal submatrices $\mathbf{A}_{11}$ and $\mathbf{A}_{22}$, depending respectively on the elementary solutions $\bar{\omega}'_{ik}$ and $\bar{\psi}''_{ik}$, are in the same order scale but, relatively to this scale, the elements of the submatrix $\mathbf{A}_{12}$, which depends on the solutions $\bar{\omega}''_{ik}$, are too large while those of the submatrix $\mathbf{A}_{21}$, which depends on the solutions $\bar{\psi}'_{ik}$, are too small. This defect of balance can be removed by preconditioning the matrix A using a diagonal $2K \times 2K$ matrix P such that:

$$\mathbf{P} = \begin{bmatrix} \mathbf{P}_{11} & 0 \\ 0 & \mathbf{P}_{22} \end{bmatrix} \tag{36}$$

The submatrices $\mathbf{P}_{11}$ and $\mathbf{P}_{22}$ are two diagonal square matrices $K \times K$. The submatrix $\mathbf{P}_{11}$ is used to decrease the elements of $\mathbf{A}_{12}$ and the submatrix $\mathbf{P}_{22}$ for increasing those of $\mathbf{A}_{21}$. The elements of $\mathbf{P}_{11}$ and $\mathbf{P}_{22}$ are calculated as follows:

$$(\mathbf{P}_{11})_{kk} = \frac{10K}{\left(\sum_{l=1}^{K} |(\mathbf{A}_{11})_{kl}| \right)}, \qquad (\mathbf{P}_{22})_{kk} = \frac{\left(\sum_{l=1}^{K} |(\mathbf{A}_{22})_{kl}| \right)}{10K} \tag{37}$$

The resulting matrix PA is well conditioned as it can be seen in *Tables 2* and *3*. Some numerical experiments have been done in order to compare the solutions obtained with and without preconditioning. For the case where the condition number of A is the worst (i.e. 8.02×10^{-6} in *Table 2*), the difference between the two solutions is about 10^{-10}%. Therefore, it can be concluded that the computations done with the system (34) are accurate. In the present case, the use of preconditioning is not really necessary. On the other hand, in other situations (large number of subdomains, interfaces in different directions), the condition number of the CI matrix becomes worse and the use of preconditioning is absolutely necessary to perform the inversion.

As already said, the elementary Stokes-type problems $\bar{P}'_{ik}$ and $\bar{P}''_{ik}$, for $i = 1, 2$ and $k = 1, \ldots, K$, are time-independent: they are solved once for all in a preprocessing stage. Hence, at each time-cycle, the two Stokes-type problems $\tilde{P}_1$ and $\tilde{P}_2$ are first solved. Then, using the various influence matrices, values of the vorticity at walls and its values as well as the ones of the stream function at the interface are calculated, so that the final values of the vorticity and the stream function at time-level $n+1$ are obtained as solution of Helmholtz equations with Dirichlet conditions. It must be pointed out that the whole algorithm reduces to the solution of Dirichlet problems for Helmholtz equations. The number of problems to be solved may be very large but only eight of them are time-dependent. All the others are solved in the precalculation stage. At last, thanks to the full diagonalization procedure, the computational effort at each time cycle reduces to matrix products. Concerning the CPU time, we observed that the cost of the preprocessing stage is equal to about 56 times the cost of one time-cycle, that is negligible when compared to the number of time cycles (up to 40,000) needed to reach the steady state solution.

The algorithm used is:

*Preprocessing stage:

(1) Construction, inversion and storage of the BI matrix for the problems $\tilde{P}_1$, $\bar{P}'_{1k}$ and $\bar{P}''_{1k}$ and for the final problem in Ω_1,

(2) Construction, inversion and storage of the BI matrix for the problems $\tilde{P}_2$, $\bar{P}'_{2k}$ and $\bar{P}''_{2k}$ and for the final problem in Ω_2.

(3) For $k=1, \ldots, K$
- Solution $(\bar{\omega}'_{1k}, \bar{\psi}'_{1k})$ of the problem $\bar{P}'_{1k}$ in Ω_1,
- Solution $(\bar{\omega}'_{2k}, \bar{\psi}'_{2k})$ of the problem $\bar{P}'_{2k}$ in Ω_2,
- → Calculation of the kth column of the CI matrix A.
- Solution $(\bar{\omega}''_{1k}, \bar{\psi}''_{1k})$ of the problem $\bar{P}''_{1k}$ in Ω_1,
- Solution $(\bar{\omega}''_{2k}, \bar{\psi}''_{2k})$ of the problem $\bar{P}''_{2k}$ in Ω_2,
- → Calculation of the $(k+K)$th column of the CI matrix A.

(4) Preconditioning of the matrix A (optional).

(5) Inversion of the CI matrix A and storage.

* At each time-cycle:

(1) - Solution $(\tilde{\omega}_1, \tilde{\psi}_1)$ of the problem $\tilde{P}_1$,
- Solution $(\tilde{\omega}_2, \tilde{\psi}_2)$ of the problem $\tilde{P}_2$,
- Calculation of the right hand side of (34).
- Multiplication by the matrix P (optional).
- Calculation of the values λ_k, μ_k for $k=1, \ldots, K$.

(2) Solution (ω_i, ψ_i), $i=1, 2$, of a problem of type $\tilde{P}_1$ or $\tilde{P}_2$ with the boundary conditions on β:

$$\begin{aligned} \omega_i(\eta_k) &= \lambda_k \\ \psi_i(\eta_k) &= \mu_k \end{aligned} \qquad \text{for } \eta_k(\pm 1, Z_k) \in \beta_c$$

INFLUENCE OF THE SINGULARITY

The change of boundary conditions at the junction C crystal-free surface induces a singularity in the vorticity ω. More precisely, for the two-dimensional plane Stokes problem, it is known that the vorticity ω behaves like $\rho^{-1/2}$, where ρ is the distance to the singular point. At the same point the azimuthal velocity derivative, as well as the temperature one in case 2, exhibits the same type of behaviour, like $\rho^{-1/2}$ for the plane Laplace equation.

Moreover, the problem is made a little more complicated by the presence of the coordinate singularity at the axis $r=0$. The numerical results given by the monodomain as well as the two-domain methods show the presence of a small oscillation for the vorticity (with a larger amplitude in the monodomain case) below the crystal at the first collocation point near the axis. Numerical experiments carried out in the two-domain configuration showed that this oscillation disappeared when the boundary singularity is removed (noslip condition on the whole boundary) or if the symmetry axis $r=0$ is discarded by inserting an inner radius $r_s=0.01$. The same experiment (inserting an inner radius) on the monodomain configuration showed that the oscillation decreases but does not disappear. From these experiments, we conclude that the oscillation is due to the interaction between the singularity at the junction C and the coordinate singularity at $r=0$, the influence of the singular point C being more important in the monodomain case. This oscillation completely disappears in the multidomain solution when introducing a coordinate transformation in Ω_1 in order to put the collocation points away from the axis. The

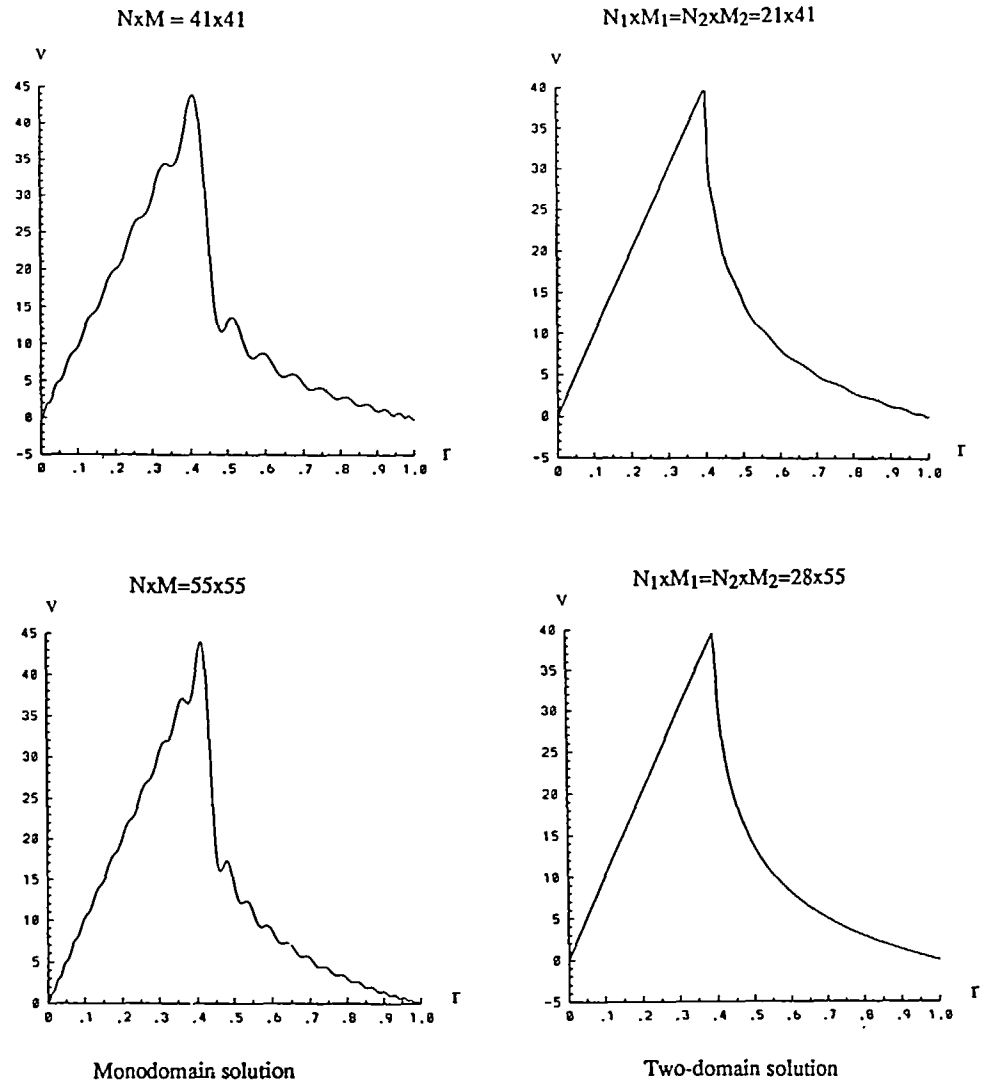

Figure 5 Azimuthal velocity profile on the crystal-free surface boundary for $Re_x = 100$ and $Gr = 0$

chosen coordinate transformation is:

$$y = 2\left(\frac{Y+1}{2}\right)^{1/2} - 1, \quad -1 \leqslant Y \leqslant 1 \tag{40}$$

The multidomain results presented below for the case $Re_x = 100$ and $Gr = 0$ were obtained with this coordinate transformation.

As already mentioned, the change in boundary conditions on the crystal and on the free surface induces a singularity of the azimuthal velocity derivatives. *Figure 5* presents the profiles of v interpolated on a regular mesh with 201 points, using the Chebyshev polynomial interpolation. We can see that the two-domain solution is already acceptable (it presents only little oscillations on the free surface) for the resolution 41×41 while the monodomain solution exhibits large

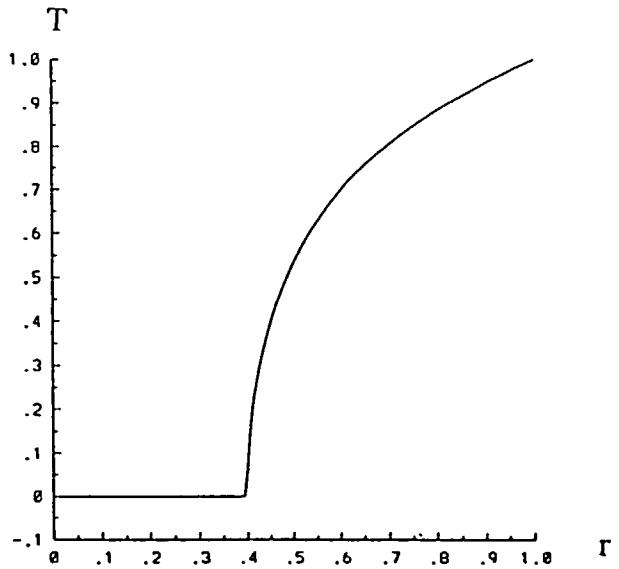

Figure 6 Temperature profile on the crystal-free surface boundary for case 2 and $Re_x = 100$, $Gr = 0$ ($N \times M = 41 \times 41$)

oscillations. For the resolution 55×55, there are no oscillation on the multidomain profile but there are still on the monodomain one. The behaviour of v is responsible of many problems for the monodomain solution as large Gibbs oscillations on the profile of the tangential derivative on and under the boundary, and an overestimate of the maximum of the normal derivative on the boundary. All these anomalies do not appear on the two-domain solution.

Let us note that the same difficulties are encountered for the temperature (in case 2) with the monodomain method as those encountered for the azimuthal velocity. Indeed, the temperature exhibits a infinite derivative at point C, as it can be seen on the temperature profile (*Figure 6*) for the two-domain solution interpolated on the 201-points regular mesh.

Figures 7a and *7b* show the vorticity profile on the boundary crystal-free surface for the monodomain and the two-domain solutions. We see that the singularity is much better described with the two-domain method. The unability of the monodomain method to capture correctly the solution is clearly visible on the profile of the solution interpolated on 201 equispaced points: this profile exhibits great oscillations, in particular near the axis (see *Figure 7c*). For the multidomain solution, the interpolation is done independently in each subdomain. So, the interpolation in Ω_1 necessitates the value of ω at the corner (1, 1), that is at the singular point. Theoretically, the vorticity is infinite at this point but numerically, it cannot be obtained. That is why no interpolated two-domain profiles on the boundary crystal-free surface are presented here. The vorticity profile below this boundary (at $Z = 0.995$) for the monodomain and for the two-domain solutions interpolated on the 201-points mesh are represented in *Figure 8*. The superiority of the two-domain solution is clearly visible.

All the discontinuities increase with Re_x. In order to solve the difficulties encountered for v and ω with the monodomain method, we tried to close up the mesh in the critical passage by increasing the degree of the approximation but all the observed defaults increased with the resolution, except the oscillations on the vorticity profile at $Z = 0.995$ that decrease but have not disappeared for the resolution 65×65 (see *Figure 8*). On the other hand, for the multidomain solution, these oscillations decrease rapidly when the resolution is increased and disappear completely for $N_1 \times M_1 = N_2 \times M_2 = 33 \times 65$.

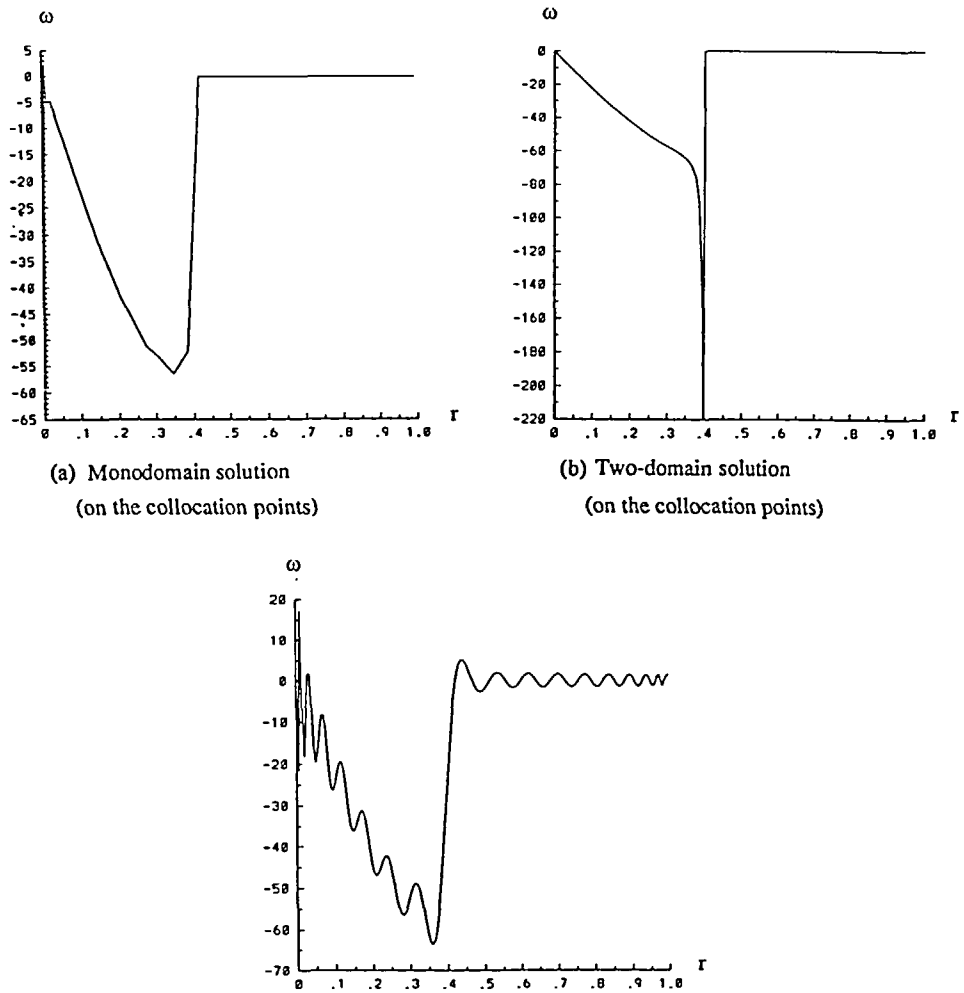

(a) Monodomain solution (on the collocation points)

(b) Two-domain solution (on the collocation points)

(c) Interpolated monodomain solution (on 201 equispaced points)

Figure 7 Vorticity profile on the crystal-free surface boundary for $Re_x=100$ and $Gr=0$. (Monodomain case: $N\times M=41\times 41$, Two-domain case: $N_1\times M_1=N_2\times M_2=21\times 41$)

Therefore, it is clear that the monodomain method is not adapted to the problem considered here. The representation of a solution exhibiting an "inner" singularity with a single polynomial leads to large Gibbs-type oscillations which cannot be removed by increasing the resolution. On the other hand, by splitting the computational domain into two subdomains just at the junction crystal-free surface, we isolate the singularity at a corner of subdomains. Then, the solution is represented by two local polynomials free of oscillations. However, a deeper study of the numerical accuracy is necessary to know the real efficiency of the multidomain method.

It is well known that the main advantage of the Chebyshev approximations is their high precision. More precisely, for functions having α continuous derivatives, the order of the error is $1/N^{\alpha}$ where N is the degree of the polynomial approximation. For an indefinitely differential function α is greater than any positive integer: it is the spectral accuracy. In the present problem,

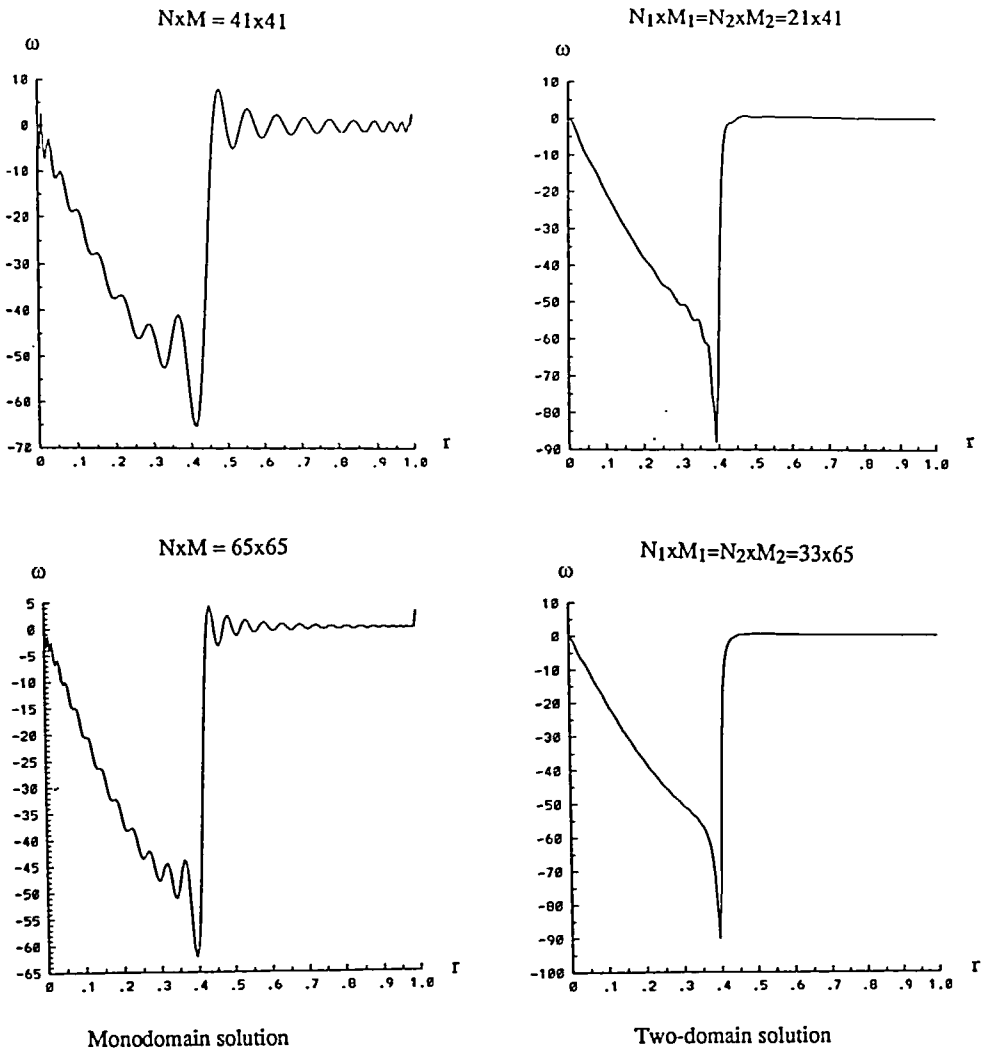

Figure 8 Vorticity profile below the crystal-free surface boundary (at $Z=0.995$) for $Re_x=100$ and $Gr=0$

the existence of singularities forbids such an accuracy, especially in the monodomain case. It is interesting to determine the degree of accuracy by examining the decay of the spectral coefficients. *Figure 9* shows the spectral coefficients $a_k(z)$ of the vorticity on two lines of collocation points $Z=Z_1$ and $Z=Z_4$ under the crystal-free surface boundary. For the resolution 65×65 in the monodomain case or $2\times(33\times65)$ in the multidomain one, these points are very close to the singular points since $Z_4=0.981$. Analogous spectra in the radial Y-direction near the interface ($Y=Y_4=0.924$ in Ω_1 and $Y=Y_{N_2-3}=-0.924$ in Ω_2) are shown in *Figure 10*. From these various spectra, it can be concluded that the decay of the absolute values of the coefficients outside a small neighbourhood of the singular point ensures the accuracy of the two-domain solution. This is not the case for the monodomain solution.

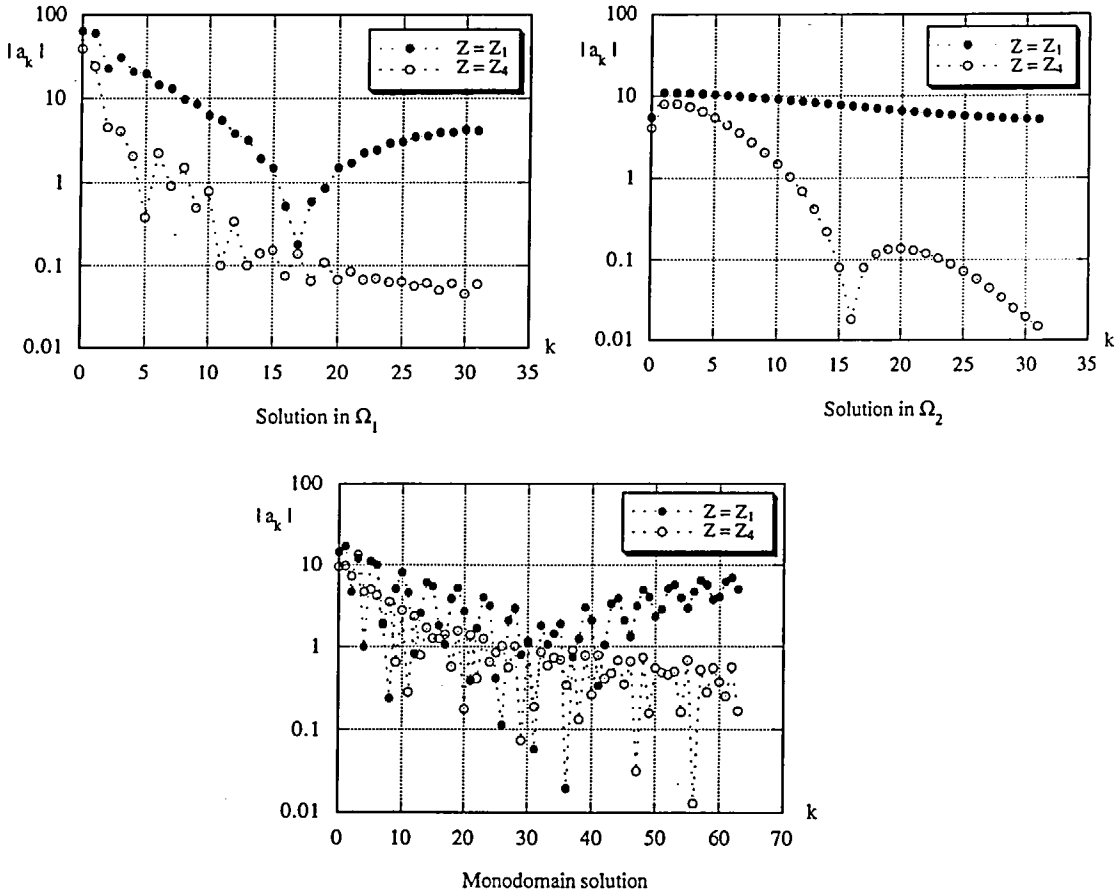

Figure 9 Vorticity spectral coefficients on different lines of collocation points in the axial direction near the singularity ($N \times M = 65 \times 65$)

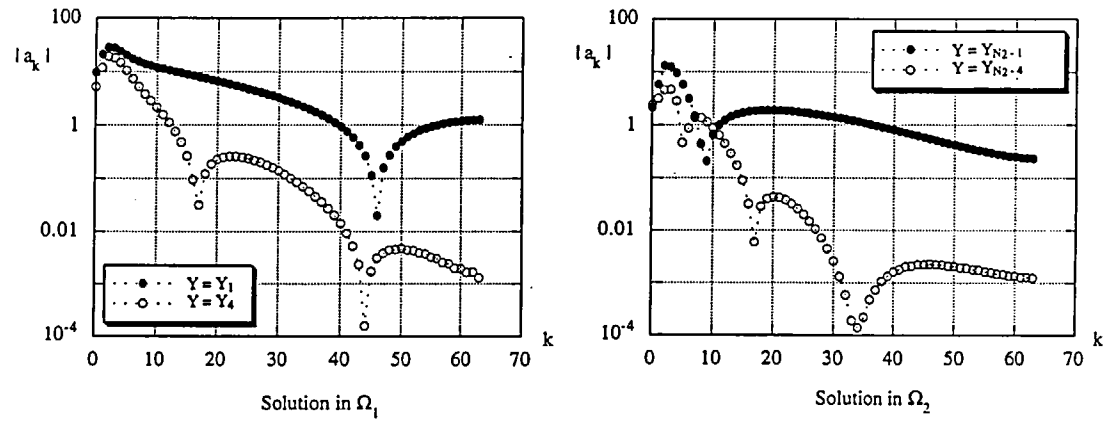

Figure 10 Vorticity spectral coefficients on different lines of collocation points in the radial direction near the singularity ($N \times M = 65 \times 65$)

COMPUTATIONAL ASPECTS

All the computations presented here have been done with the gap ratio $\alpha=1$, the radius ratio $\gamma=0.4$ and the Prandtl number $Pr=0.05$. In order to compare the multidomain and the monodomain solutions we define the following characteristic variables: ψ_{max}, the maximum value of ψ; ψ_{min}, the minimum value of ψ; $|V|_{max}$, the maximum value of the velocity modulus in the meridian plane ($|V|=(u^2+w^2)^{1/2}$); $Res\phi$, the residual on ϕ defined by:

$$Res\phi=(sup|3\phi^{n+1}(Y_j, Z_i)-4\phi^n(Y_j, Z_i)+\phi^{n-1}(Y_j, Z_i)|)/2\delta t \quad \text{for } \phi=T, v$$

and by:

$$Res\phi=(sup|3\phi^{n+1}(Y_j, Z_i)-4\phi^n(Y_j, Z_i)+\phi^{n-1}(Y_j, Z_i)|)/(2\delta t|\phi|_{max}) \quad \text{for } \phi=\omega,$$

where Y_j, Z_i are the collocation points in the two spatial directions and δt is the time-step. It must be noted that the maxima and minima are calculated on the collocation points. We are conscious that, consequently, the comparison will not be very precise since the location of the collocation points is not the same in the monodomain and in the two-domain cases for the same resolution.

The details of the computations are given in *Tables 4* and *5*. The last column refers to the initial condition. For each value of the Reynolds number Re_x, the initial condition is given either by the solution (9) or by the solution obtained for a previous value of Re_x. All results presented here correspond to the thermal boundary condition of case 1.

The used time-step δt varies from 10^{-2} to 5×10^{-6} for the monodomain solution and from 10^{-2} to 10^{-5} for the two-domain one according to the values of Gr, Re_x, and to the spatial resolution. *Table 6* gives time-steps δt_1 and δt_2, for different values of Gr and Re_x, so that the critical time-step δt_c verifies $\delta t_1 \leqslant \delta t_c < \delta t_2$. We note that, when Re_x increases, the critical time-step is smaller for the monodomain method than for the multidomain method.

On the Cray YMP2E computer, the computational cost for one time-cycle is 0.024 s in the monodomain case and 0.039 s in the two-domain case, for the same resolution $N\times M=41\times41$ (in the multidomain case $N_1=N_2=(N+1)/2$). So the multidomain method is not much more time-consuming than the monodomain method. More, for some cases, the number of modes necessary to have a good representation of the solution with the monodomain method can become very large ($N\times M=55\times73$ for $Gr=10^5$ and $Re_x=2000$). For such a resolution the computational cost for one time-cycle can reach 0.071 s, and the convergence towards the steady state necessitates more time-cycles than in the multidomain case.

It has been observed that the convergence towards the steady state is slower for the azimuthal velocity than for the other variables (in both monodomain and two-domain cases). Therefore, taking into account the fact that the ultimate states were known to be steady, a larger time-step was used for v in some cases. Let us note at last that the computation is stopped when the residual on v decays below a required value, $Resv<10^{-6}$.

ANALYSIS OF THE FLOWS

This closing section is devoted to a comparison of the monodomain and the two-domain methods for various values of Re_x (rotation of the crystal) and Gr (intensity of the heating). In the same time the flow configuration according to these values is described. Thermal boundary conditions of type 1 have been used in all the computations. The spatial resolution is 41×41 for the monodomain case and $2\times(21\times41)$ for the two-domain one. At last, let us note that the coordinate transformation (40) has not been used for the calculations discussed in the present section.

First, the effect of the rotation only was studied ($Gr=0$). It is observed, when Re_x increases from 100 to 1000, that the centre of the cell is rejected under the free surface of the melt by the more rapid rotation of the crystal. The shear of the azimuthal velocity is magnified and the shear layer for $Re_x=1000$ is much more concentrated under the crystal. Concerning the

Table 4 List of the runs for $Gr=0$

Domains	N × M	*Rex*	ψ_{max}	ψ_{min}	$\|V\|_{max}$	δt	*Nc*	*Resω*	*ResT*	*Resv*	Initial condition
1	41 × 41	100	4.37×10^{-6}	−0.200	4.29	10^{-2}	300	10^{-9}	10^{-12}	10^{-10}	sol. (9)
	51 × 51		4.16×10^{-6}	−0.187	4.10	10^{-2}	300	10^{-9}	10^{-12}	10^{-9}	sol. (9)
	61 × 61		5.24×10^{-6}	−0.221	4.48	10^{-2}	400	10^{-9}	10^{-12}	10^{-9}	sol. (9)
	73 × 73		5.01×10^{-6}	−0.213	4.38	10^{-2}	450	10^{-9}	10^{-12}	10^{-9}	sol. (9)
2	41 × 41	100	4.85×10^{-6}	−0.224	4.46	10^{-2}	200	10^{-10}	10^{-11}	10^{-10}	sol. (9)
	49 × 41		4.68×10^{-6}	−0.225	4.46	10^{-2}	200	10^{-10}	10^{-11}	10^{-10}	sol. (9)
	49 × 49		4.81×10^{-6}	−0.225	4.46	10^{-2}	200	10^{-10}	10^{-11}	10^{-10}	sol. (9)
1	41 × 41	1000	7.12×10^{-5}	−4.612	72.85	2×10^{-5}	4000	10^{-7}	10^{-9}	10^{-7}	$Rex=100$, $Gr=0$ (41 × 41)
2	41 × 41	1000	7.89×10^{-5}	−5.074	89.76	10^{-4}	16,000	10^{-8}	10^{-9}	10^{-8}	$Rex=100$, $Gr=0$ (41 × 41)

N_c is the Number of time-steps necessary to reach convergence.
In the case of 2 domains, we have $N_1=N_2=(N+1)/2$.

Table 5 List of the runs for $Gr=10^5$

Domains	N × M	*Rex*	ψ_{max}	ψ_{min}	$\|V\|_{max}$	δt	*Nc*	*Resω*	*ResT*	*Resv*	Initial condition
1	41 × 41	10	28.55	-2.29×10^{-4}	190.14	5×10^{-5}	27,000	10^{-7}	10^{-9}	10^{-9}	sol. (9)
2	41 × 41	10	28.39	-1.19×10^{-5}	189.81	5×10^{-5}	20,000	10^{-7}	10^{-9}	10^{-9}	sol. (9)
1	41 × 41	100	28.52	-2.28×10^{-4}	189.88	2×10^{-5}	35,000	10^{-6}	10^{-9}	10^{-7}	$Rex=10$, $Gr=10^5$ (41 × 41)
2	41 × 41	100	28.36	-1.20×10^{-5}	189.53	5×10^{-5}	20,000	10^{-7}	10^{-9}	10^{-7}	$Rex=10$, $Gr=10^5$ (41 × 41)
1	41 × 41	1500	21.21	−1.826	145.91	10^{-5}	50,000	10^{-6}	10^{-8}	10^{-6}	$Rex=100$, $Gr=10^5$ (41 × 41)
2	41 × 41	1500	18.25	−2.510	128.65	2×10^{-5}	38,000	10^{-8}	10^{-9}	10^{-6}	$Rex=1000$, $Gr=10^5$ (41 × 41)
2	41 × 41	1850	9.34	−4.501	159.73	2×10^{-5}	40,000	10^{-8}	10^{-9}	10^{-7}	$Rex=1700$, $Gr=10^5$ (41 × 41)
1	41 × 41	2000	12.48	−4.058	141.36	8×10^{-6}	60,000	10^{-6}	10^{-8}	10^{-6}	$Rex=1500$, $Gr=10^5$ (41 × 41)
	51 × 51		13.76	−3.806	139.21	8×10^{-6}	80,000	10^{-6}	10^{-8}	10^{-6}	$Rex=2000$, $Gr=10^5$ (41 × 41)
	55 × 61		10.99	−4.310	142.87	5×10^{-6}	164,000	10^{-5}	10^{-8}	10^{-6}	$Rex=2000$, $Gr=10^5$ (55 × 55)
	55 × 73		10.91	−4.325	143.29	5×10^{-6}	143,000	10^{-6}	10^{-8}	10^{-6}	$Rex=2000$, $Gr=10^5$ (55 × 61)
2	41 × 41	2000	3.58	−5.271	175.53	2×10^{-5}	80,000	10^{-8}	10^{-9}	10^{-6}	$Rex=1500$, $Gr=10^5$ (41 × 41)
	49 × 49		3.56	−5.264	175.89	10^{-5}•	92,000	10^{-7}	10^{-8}	10^{-6}	sol. (9)
	55 × 61		3.54	−5.295	175.94	5×10^{-6}•	175,000	10^{-7}	10^{-8}	10^{-6}	sol. (9)
1	41 × 41	2500	1.59	−6.586	179.59	5×10^{-6}	120,000	10^{-7}	10^{-8}	10^{-6}	$Rex=2050$, $Gr=10^5$ (41 × 41)
2	41 × 41	2500	1.65	−7.698	229.15	10^{-5}*	57,000	10^{-8}	10^{-9}	10^{-6}	$Rex=2050$, $Gr=10^5$ (41 × 41)
2	41 × 41	3000	0.622	−9.741	279.26	10^{-5}•	55,000	10^{-7}	10^{-8}	10^{-5}	$Rex=2500$, $Gr=10^5$ (41 × 41)

*The time-step used for v is $\delta t_v=5\delta t$ from the 50,000th cycle to accelerate the convergence.
•The time-step used for v is $\delta t_v=2\delta t$ from the 50,000th cycle to accelerate the convergence.

Table 6 Values of the time-steps such as $\delta t_1 \leqslant \delta t_c < \delta t_2$ for different values of *Gr* and *Rex* ($N \times M = 41 \times 41$ with $N_1 = N_2 = (N+1)/2$ in the two-domain case)

Domains	*Gr*	*Rex*	δt_2	δt_1
1	0	100	2×10^{-2}	10^{-2}
2	0	100	2×10^{-2}	10^{-2}
1	0	1000	5×10^{-5}	2×10^{-5}
2	0	1000	2×10^{-4}	10^{-4}
1	10^5	10	10^{-4}	5×10^{-5}
2	10^5	10	10^{-4}	5×10^{-5}
1	10^5	100	5×10^{-5}	2×10^{-5}
2	10^5	100	8×10^{-5}	5×10^{-5}
1	10^5	2500	6×10^{-6}	5×10^{-6}
2	10^5	2500	2×10^{-5}	10^{-5}

temperature, it can be seen that the isotherm patterns do not change very much when increasing Re_x: they reflect conduction. Note that the monodomain azimuthal velocity exhibits oscillations on the free surface of the melt and at the vertical of the singular point (*Figure 11*).

Then, the coupled convection with $Gr = 10^5$ was considered. For $Re_x < 1000$, the basic cell is dominated by convection and concentrated in the bottom of the crucible. The azimuthal velocity undergoes the diffusion: a maximum value appears inside the domain. It can be noted here again that the monodomain patterns exhibit oscillations on the free surface. The isotherm patterns are not shown for this case because no difference between monodomain and multidomain solutions is visible. However, it has been observed that their great distortion near the heated wall of the crucible reflects the effect of the thermal transport: it is the natural convection which dominates the flow. It is interesting at last to look at the iso-vorticity patterns, drawn on the collocation points (*Figure 12*): it can be noted that the monodomain solution exhibits oscillations at the vertical of the singular point, in the middle of the computational domain, whereas the two-domain one does not. Hence, the vorticity computed by the monodomain method is really not good. Yet, the flow configuration obtained with the two methods is the same. For $Re_x = 1000$, a region where there is no meridian motion appears under the crystal. Then, when Re_x is increased from 1000 to 1500, a second cell, contra-rotative to the cell induced by the thermal convection, is created in this region by the rotation of the crystal. In the region below the crystal, the fluid is dominated by the rotation, whereas, in the external zone, the thermal convection decreases. The distortion of the isothermal patterns becomes less marked. By increasing the rotation (Re_x varies from 1500 to 2000), the flow configuration changes. It is important to note that it is completely different according to the method used. For the two-domain solution, the cell induced by the rotation of the crystal increases and reaches the same intensity of the cell induced by convection for $Re_x = 1850$. The configuration of azimuthal velocity is mainly governed by a shear layer under the crystal which is more and more concentrated as Re_x increases. For $Re_x = 2000$, forced convection dominates the flow, the cell due to the rotation is predominant and the isotherm patterns are no more distorted by thermal convection (*Figure 13*). For the monodomain solution, the cell induced by natural convection is yet predominant for $Re_x = 2000$, the isotherm patterns still reflect convection (*Figure 13*), and for $Re_x = 2050$, forced convection and thermal convection balance perfectly. For $Re_x > 2050$, the cell induced by the thermal convection is more and more concentrated in the external corner in the bottom of the crucible and decreases slowly until it becomes only a nucleus for $Re_x = 3000$. Let us note that, since $Re_x = 2500$, the flow configuration is the same again with the two methods (*Figure 14*). The phenomenon goes with the disappearance of the distortion of the isotherm patterns which exhibit on the other hand a vertical stratification under the crystal more and more important as Re_x increases.

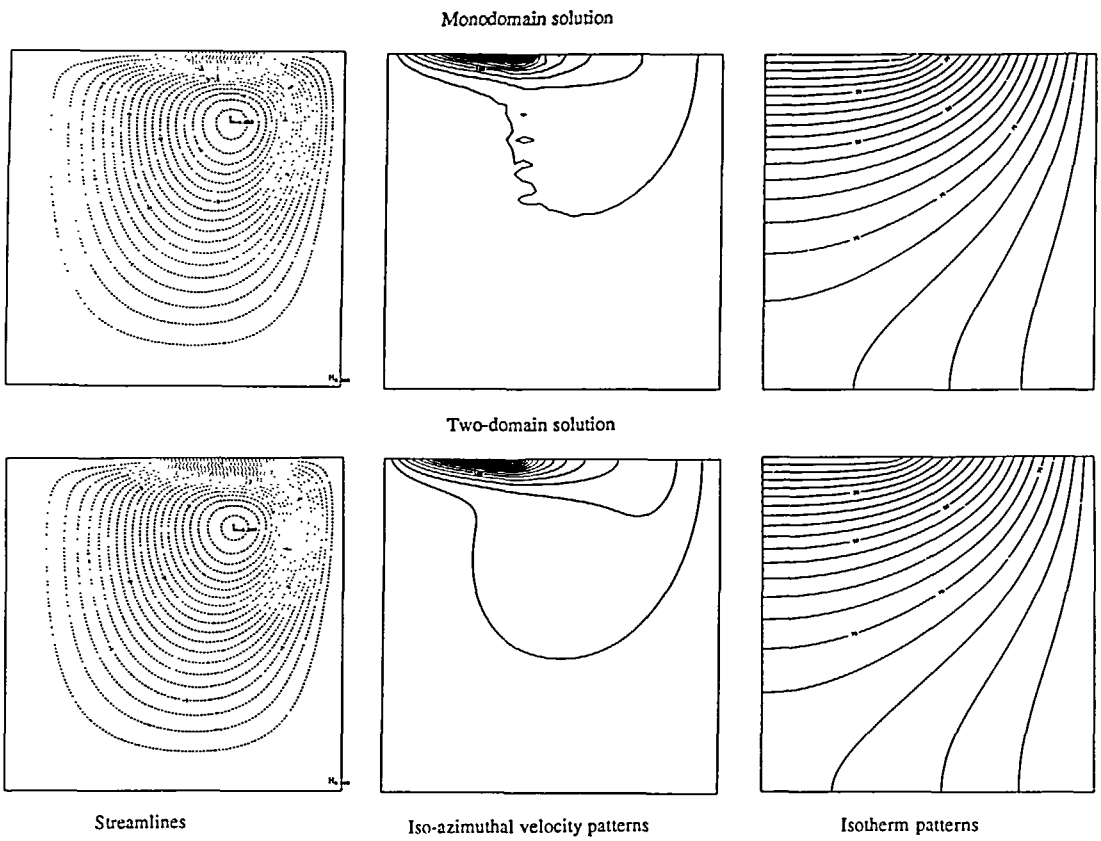

Figure 11 Flow configuration for $Re_x = 1000$ and $Gr = 0$

It is interesting to point out the difference of the onset of domination of the forced convection obtained with the two methods. As already noted, we do not obtain the same solution for $Re_x = 2000$ (*Figure 13*). Here again, it is clear that the monodomain method is not adapted to the considered problem. The loss of accuracy leads not only to oscillations but also, and this is much more important, to a shift of the threshold. This last point has been often observed when the computed solution is singular.

CONCLUSION

Through a physical problem which exhibits singularities at a boundary of the domain, the Czochralski crystal growth technique, it has been shown that a global approximation with a spectral method gives very poor results in terms of accuracy, presenting in particular very large oscillations and changing the threshold between two types of flow patterns.

These drawbacks have been removed by introducing a multidomain technique. The idea was to work in two separate domains so that the singularity is isolated at a corner. Then the solution is represented by two local different polynomials. The solution method makes an extensive use of the influence matrix technique for the prescription of the matching conditions at the interface as well as the boundary conditions on the physical boundaries. The method is direct and requires only matrix products at each time-cycle, leading to a very efficient numerical code.

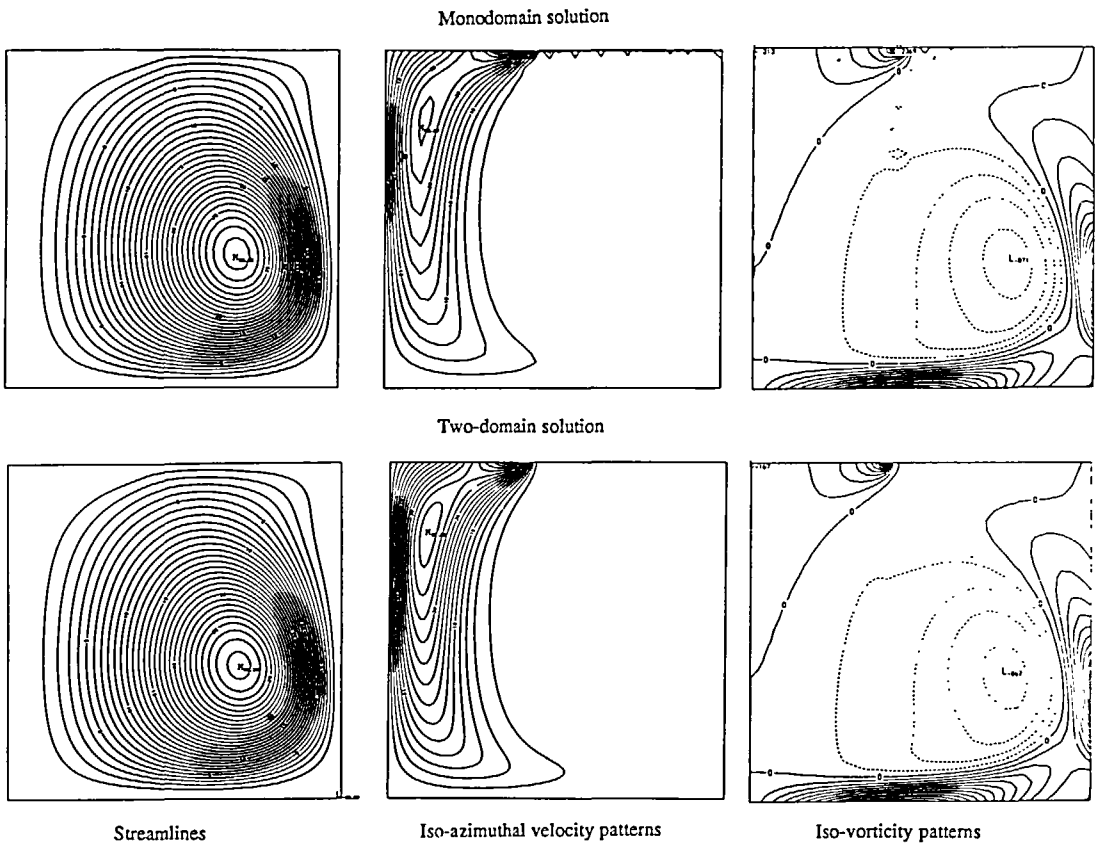

Figure 12 Flow configuration for $Re_x = 100$ and $Gr = 10^5$

ACKNOWLEDGEMENTS

The authors would like to thank Dr P. Bontoux, Dr A. Randriamampianina, and Ph. Larroudé for useful discussions. They also gratefully acknowledge support from the *Direction des Recherches, Etudes et Techniques,* from the *Conseil Régional Provence-Alpes-Côte d'Azur* (through the *Centre Régional de Calcul Scientifique de l' Institut Méditerranéen de Technologie*) and from CNRS (through IDRIS Computing Center). They acknowledge emulating collaborations inside GDR 'MFN' CNRS research group.

REFERENCES

1 Basdevant, C., Deville, M., Haldenwang, P., Lacroix, J. M., Ouazzani, J., Peyret, R., Orlandi, P. and Patera, A. T. Spectral and finite difference solutions of Burgers equation, *Computers and Fluids*, **14**, 23–41 (1986)
2 Guillard, H. and Peyret, R. On the use of spectral methods for the numerical solution of stiff problems, *Comp. Meth. Appl. Mech. Eng.*, **66**, 17–43 (1988)
3 Pulicani, J. P. A spectral multidomain method for the solution of 1D-Helmholtz and Stokes-type equations, *Computers and Fluids*, **16**, 207–215 (1988)
4 Lacroix, J. M., Peyret, R. and Pulicani, J. P. A pseudospectral multidomain method for the Navier-Stokes equations with application to double diffusive convection, *Proc. Seventh GAMM-Conf. Numer. Meth. Fluid. Mech.*, M. Deville, ed. (Vieweg, Braunschweig), 167–174 (1988)
5 Peyret, R. The Chebyshev multidomain approach to stiff problems in fluid mechanics, *Comp. Meth. Appl. Mech. Eng.*, **80**, 129–145 (1990)

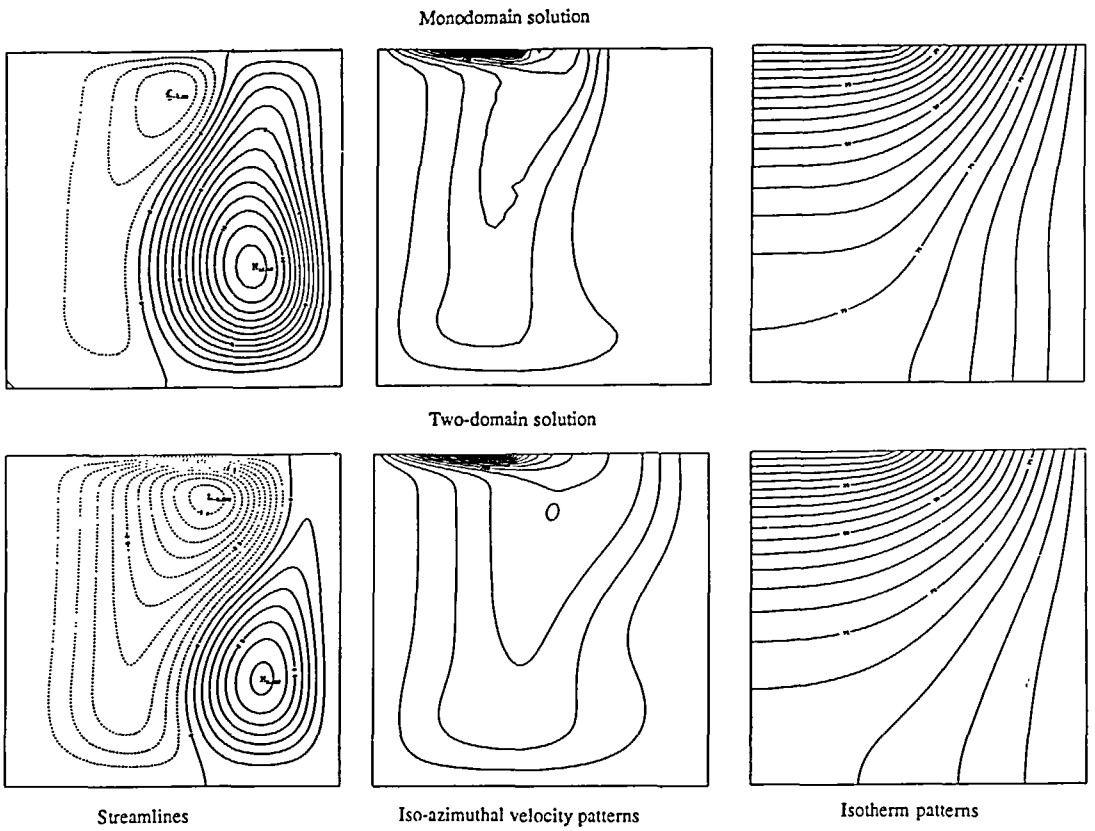

Figure 13 Flow configuration for $Re_x = 2000$ and $Gr = 10^5$

6 Macaraeg, M. and Streett, C. L. Improvements in spectral collocation through a multiple domain technique, *Appl. Numer. Math.*, **2**, 95–108 (1986)
7 Marion, Y. and Gay, B. Résolution des équations de Navier-Stokes par une méthode pseudo-spectrale via une technique de coordination, Sixth Int. Symp. on Finite Element Method in Flow Problems, Antibes, 239–243 (1986)
8 Vanel, J. M., Peyret, R. and Bontoux, P. A pseudospectral solution of vorticity-stream function equations using the influence matrix technique, *Numer. Meth. for Fluid Dynamics II*, K. W. Morton and M. J. Baines Eds. 463–475 (1986)
9 Ehrenstein, U. and Peyret, R. A Chebyshev collocation method for the Navier-Stokes equations with Application to Double-diffusive convection, *Int. J. Numer. Meth. Fluids*, **9**, 427–452 (1989)
10 Ouazzani, J., Peyret, R. and Zakaria, A. Stability of collocation-Chebyshev schemes with application to the Navier-Stokes equations, *Proc. Sixth GAMM-Conf. Numer. Meth. Fluid Mech.*, D. Rues and W. Kordulla, Eds. (Vieweg, Braunschweig 287–294 (1986)
11 Hurle, D. T. J. *Crystal Pulling from the Melt*, Springer-Verlag Berlin Heidelberg (1993)
12 Fontaine, J.-P., Randriamanpianina, A. and Bontoux, P. Numerical simulation of flow structures and instabilities occuring in a liquid-encapsulated Czochralski process, *Physics of Fluids*, **3**, 10, 2310–2331 (1991)
13 Rothman, E. Reducing round-off error in Chebyshev pseudospectral computations, *High Performance Computing II*, M. Durand and F. El Dabaghi, Eds., 423–439 North Holland, Amsterdam (1991)
14 Ouazzani, J. *Méthode pseudo-spectrale pour la résolution des équations d'un mélange de gaz binaire*, Thesis, University of Nice (1984)
15 Pulicani, J. P. *Application des méthodes spectrales à l'étude d'écoulements de convection*, Thesis, University of Nice (1988)
16 Ehrenstein, U. *Méthodes spectrales de résolution des équations de Stokes et de Navier-Stokes: Application à des écoulements de convection double-diffusive*, Thesis, University of Nice (1986)
17 Chaouche, A. *Une méthode de collocation pour la prédiction et l'analyse des écoulements et des transferts dans les milieux en rotation rapide*, Thesis, University of Aix-Marseille II (1991)

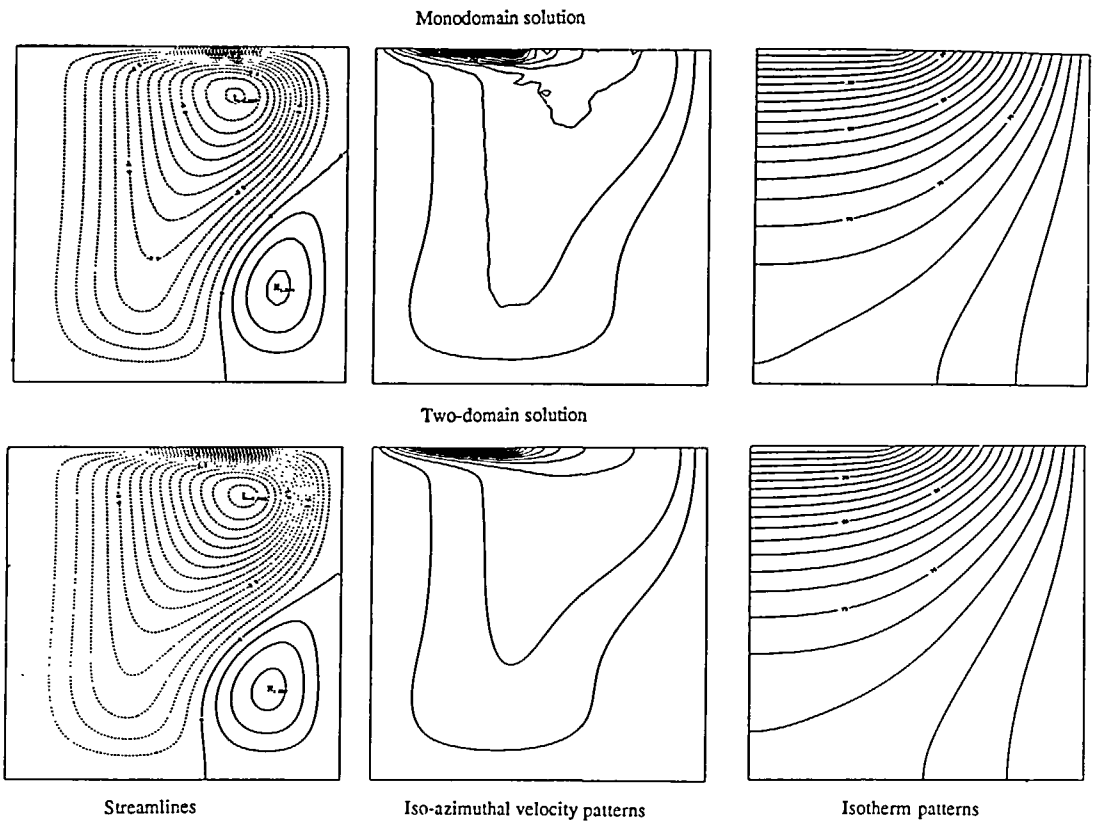

Figure 14 Flow configuration for $Re_x = 2500$ and $Gr = 10^5$

18 Bwemba, R. and Pasquetti, R. About the influence matrix used in the spectral solution of the 2D incompressible Navier-Stokes equations (vorticity-stream function formulation), *Appl. Numes. Math.*, **16**, 299–315 (1995)
19 Chan, P. F. and Resasco, B. C. A framework for the analysis and construction of domain decomposition preconditioners 1rd Int. Symp. Domain Decomoosition Methods for P. D. E. R. Glowinski *et al.* Eds, SIAM Philadelphia (1988)
20 Raspo, I. *Etude numérique de la structure d'écoulements et transfert de chaleur dans les cavités tournantes avec flux axial*, Thesis, University of Aix-Marseille II (1995)
21 Ehrenstein, U., Guillard, H. and Peyret, R. Flame computations by a Chebyshev multidomain method, *Int. J. Numer. Meth. Fluids*, **9**, 499–515 (1989)

APPENDIX

Expression of the differentiation matrix coefficients

$$d_Y^{(1)}(0, 0) = -d_Y^{(1)}(N, N) = \frac{(2N^2+1)}{6}$$

$$d_Y^{(1)}(0, k) = \frac{(-1)^k}{c_k \sin^2\left(\frac{k\pi}{2N}\right)} \qquad k = 1, \ldots, N$$

$$d_Y^{(1)}(N,k)=\frac{(-1)^{k+N+1}}{c_k\cos^2\left(\frac{k\pi}{2N}\right)} \qquad k=0,\ldots,N-1$$

$$d_Y^{(1)}(i,0)=\frac{(-1)^{i+1}}{4\sin^2\left(\frac{i\pi}{2N}\right)} \qquad i=1,\ldots,N-1$$

$$d_Y^{(1)}(i,N)=\frac{(-1)^{i+N}}{4\cos^2\left(\frac{i\pi}{2N}\right)} \qquad i=1,\ldots,N-1$$

$$d_Y^{(1)}(i,i)=-\frac{\cos\left(\frac{i\pi}{N}\right)}{2\sin^2\left(\frac{i\pi}{N}\right)} \qquad i=1,\ldots,N-1$$

$$d_Y^{(1)}(i,k)=\frac{(-1)^{i+k}}{2\sin\left(\frac{(k+i)\pi}{2N}\right)\sin\left(\frac{(k-i)\pi}{2N}\right)} \qquad i=1,\ldots,N-1,\ k=1,\ldots,N-1,\ i\neq k$$

where $c_0=c_N=2$ and $c_k=1$ for $k=1,\ldots,N-1$.